Spring 2019

Blade Design and Analysis of Horizontal-Axis Wind Turbine: CFD and Experimental Investigation of Blades Design

Relwinde Fabrice Zongo

Follow this and additional works at: https://digitalcommons.georgiasouthern.edu/etd

Part of the Energy Systems Commons

BLADE DESIGN AND ANALYSIS OF HORIZONTAL-AXIS WIND TURBINE: CFD AND

EXPERIMENTAL INVESTIGATION OF BLADES DESIGN

by

RELWINDE FABRICE WILFRIED ZONGO

(Under the Direction of Mosfequr Rahman)

ABSTRACT

The present thesis focuses on the investigations of the computational fluid dynamics analysis and the experimental study of small scales Horizontal Axis Wind Turbine (HAWT) blades. The initial steps are taken; in the process of this research were the selection of the airfoil type to be used in each blade design and the creation of a blade design with high efficiency operating in a low wind speed zone. For the mentioned blade design process, the following airfoils were selected respectively NACA 0010, NACA 0012, NACA 1412, NACA 2412, NACA 2414, NACA 4412 and NACA 6412. This selection intends to provide each blade with a greater lift force, as well as an increase in the Tip Speed Ratio (TSR). An angle of attack (AOA) 10°, 20°, and 30° are added to each blade design with reference to the longitudinal hub axis. Using the CFD software Fluent and FEA a structural analysis and computational fluid dynamic simulations were performed on one hand in order to confirm that the design is structurally sounded and on the other hand, to predict the theoretical aerodynamic performance of the blades. Eight different models of blades were designed and fabricated to conduct the experimental study, using a wind tunnel and data acquisition system to determine the performance of each blade at different wind speeds and different angles of attacks. Analyzing the results from the experimental part of the research using MATLAB indicates a significant improvement of the blade efficiency. At an optimum angle of attack between 8 degrees and 12 degrees, a minimum wind speed of 8 m/s, and an angle of twist of 17.5 degrees, the turbine generated 357 mW with a calculated improved efficiency of 24.5%.

INDEX WORDS: Horizontal-axis wind turbine, HAWT, Lift coefficient, Drag coefficient, Wind tunnel, Computational fluid dynamics, CFD, ANSYS Fluent

BLADE DESIGN AND ANALYSIS OF HORIZONTAL-AXIS WIND TURBINE: CFD AND

EXPERIMENTAL INVESTIGATION OF BLADES DESIGN

by

RELWINDE FABRICE WILFRIED ZONGO

B.S., Georgia Southern University, 2016

A Thesis Submitted to the Graduate Faculty of Georgia Southern University in

Partial Fulfillment of the Requirements for the Degree

MASTER OF SCIENCE

STATESBORO, GEORGIA

BLADE DESIGN AND ANALYSIS OF HORIZONTAL-AXIS WIND TURBINE: CFD AND

EXPERIMENTAL INVESTIGATION OF BLADES DESIGN

by

RELWINDE FABRICE WILFRIED ZONGO

Major Professor: Mosfequr Rahman

Committee: Valentin Soloiu

Marcel Ilie

Electronic Version Approved
May 2019

DEDICATION

This work is dedicated to my Family for their endless support in all of my endeavors. In addition, I would like to mentioned Wayman Parker and Emma Parker, as they have become my family away from home for their kindness and tremendous support.

ACKNOWLEDGMENTS

I would like to extend my gratitude to Dr. Mosfequr Rahman for his guidance and direction throughout my research in his wind energy laboratory. I want to thank also Dr. Marcel ILie and Dr. Valentin Soloiu for taking the time to be a part of my thesis committee and reviewing this work. I also want to thank Travis Salyers and Emile Maroha for the work they have done in the wind energy lab. Also, it is worth mentioning all the undergraduate student that has contributed to the lab throughout the semesters

TABLE OF CONTENTS

LIST OF SYMBOLS

A	Swept Area (m^2)
CFD	Computational Fluid Dynamics
C_m	Moment Coefficient
C_p	Power Coefficient
D	Blade Diameter (m)
H	Blade Height (m)
N	Rotations per Minute
TSR	Tip-Speed Ratio
T	Torque ($N\text{-}m$)
V	Wind Velocity (m/s)
VAWT	Vertical-Axis Wind Turbine
ρ	Air Density (kg/m^3)
ω	Angular Velocity (rad/s)
λ	Tip-Speed Ratio

LIST OF TABLES

LIST OF FIGURES

CHAPTER 1

INTRODUCTION

1.2 Problem Statement

As the other sources of energy create more and more undesirable side effects in the environment, wind energy is coming to the forefront as a potential source of clean renewable energy. In other terms, it is to believe that the need for everlasting alternative energy sources is ever prevalent. Wind energy is one of the most viable renewable sources today due to its year-round availability, and pollution-free nature. According to the *Wind Vision Report*, published by the U.S. Department of Energy, wind energy is the largest source of added renewable energy generation in the United States since 2000. A plan has been set by the program for 20% of the nation's electricity to be supplied by wind by the year 2030, and 35% by 2050. The report states that a key to achieving this goal is to improve the potential of low-wind-speed locales (ENERGY.GOV, 2016). Due to this, numerous works are underway involving the efficiency of wind energy conversion systems, especially for regions with low average wind velocities. It is important to mention that there are two primary types of conversion systems of wind energy: the horizontal-axis wind turbine (HAWT) and the vertical-axis wind turbine (VAWT). HAWTs have been in practice for some time and are heavily favored over VAWTs for large-scale power generation.

1.3 History of Wind Energy

History is teaching us that for many years' people have used the wind to propel their boats and this has laid the use of wind for mechanical and electrical purposes. In the 1st century AD, for the first time the wind-driven wheel was developed and the inventor of this technique is known to

be a Greek engineer, Heron of Alexandria. By the 7th to the 9th century, wind wheels had been spread out to other parts of the world. For instance, in the sustain region of Iran, the technique of wind wheels was used for practical purposes. In the same way, the technique of wind wheel was reconverted in windmills which were used to grind corn, grind flour and pump water. Yet, as the technique continued to spread out, by 1000 AD windmills were being used in China and Sicily to pump seawater to make salt. It was then, around 1887 that the first wind turbine was invented and built in Scotland in order to produce electricity. Indeed, the inventor of the wind turbine was James Blyth. The invention was 10 m high and was used to charge accumulators and electricity supply of the neighbors. It will be years later, precisely in 1931, in Yalta that the first horizontal axis wind turbines were built and were delivering around 100 KW of capacity, with a 32% load factor. Since then and with the dynamic of the scientific revolution the wind energy idea has not stopped evolving. In 1975 Johannes Juul successfully built a HAWT with a diameter of 24 meters and 3 blades and his wind turbine is believed to be very similar in design to the one being used nowadays. The particularity of this design was the use of aerodynamic techniques.

Figure 1.1. Jacobs turbine (Jacobs 1961)

In summary, it is important to note that wind turbines are devices that can be used to convert kinetic energy from the wind to electrical power, mainly using a mechanical rotor, a drive train, and a generator. The history books revealed that the first wind turbine was designed by Paul La Cour, who was a professor in Denmark in 1891. Since then, his idea has evolved and today the largest wind turbine (Enercon E-126) generates 7 megawatts of power under a rated speed. With new technology, there are existing modern wind turbines that can be mounted either on the ground or on the seabed like in Norway where an offshore wind turbine of 10 megawatts was installed in 2011. As the other sources of energy create more and more undesirable side effects in the environment, wind energy is coming to the forefront as a potential source of clean renewable energy.

Figure 1.2. Paul La Cour electricity producing wind turbine in 1891.

1.4 Modern Wind Turbines

A wind turbine is known as a mechanism that converts the power in the wind into electricity. In contrast to a windmill, the second one converts wind power into mechanical power. In the modern days, the wind turbines are an electrical network that is constituted of a battery-charging circuit, residential scale power systems, isolated or island networks, and large utility grids. In a modern wind turbine, the conversion process utilizes the basic aerodynamic force of lift, to produce a positive torque on the rotating shaft. This shaft rotation results at first by the production of power called mechanical power and is then followed by the generation of electricity in the incorporated generator. In recent years, the horizontal axis wind turbine (HAWT) is the most commonly used wind turbine design. In the case of HAWT, it is important to notice that the axis of rotation is parallel to the ground. The common HAWT are designed with a subsystem, which can be decomposed in the following:

● A rotor: a system consisting of the blade and the supporting hub.

● A drive train: a mechanism composed with rotating parts of a turbine, not including a rotor. In that system, the shafts, the gearbox, coupling, a mechanical, and the generator can be included.

● A tower and the foundation

● A mechanical control

● An electrical system: cables, switchgear, transformers, and power converters.

The above horizontal axis wind turbine subsystem is illustrated in Figure 1.2.
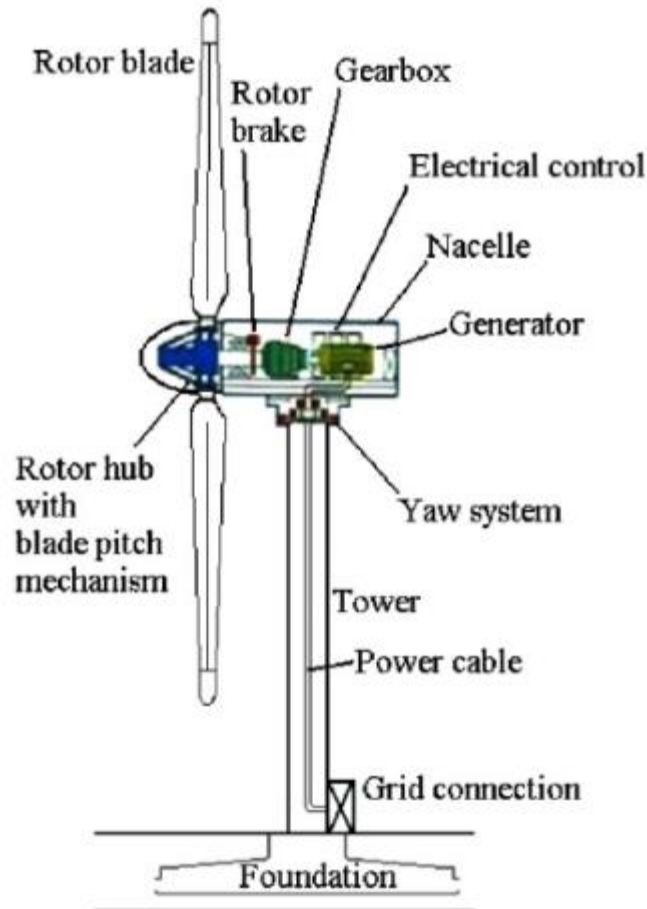
Figure 1.3. Common configuration of HAWT system (Research gate, 2017)

1. 5 HAWT Advantages

The horizontal axis wind turbine (HAWT) can be defined as a turbine whose axis of rotation is parallel to both the wind flow and the ground. Generally, HAWT has two or three blades, and there are two main kinds of HAWT: upwind and downwind. An upwind turbine can be described as a turbine where the rotor faces the wind, and this kind of mechanism requires the use of a yaw mechanism in order to keep the rotor facing the wind at all times. On the other hand, a downwind turbine is slightly different from the upwind turbine because the rotor faces the downwind side of the tower. This mechanism does not need a yaw mechanism because the rotors are designed to be more flexible.

1.6 HAWT Disadvantages

Several studies have proven that horizontal wind turbines are very functional and efficient. However, a certain number of factors in the construction and the entire technology behind the system of HAWT can be extremely expensive, and the transport and the installation can be very challenging. Also, because the horizontal axis wind turbine installation necessitates the use of a high altitude tower this can be seen as desirable for certain landscape. Besides all the difficulties mentioned above, it is critical to point out that the horizontal wind turbine, if used with a downwind machine, is subject to very low efficiency because the HAWT cannot withstand the turbulence fatigue. Another disadvantage of the HAWT comes from the fact that maintenance can be very difficult and this is due to the fact that the gearbox, generator and the rotor are all located at the top of the very tall tower. Conventional horizontal axis wind turbine rotors with one, two and three blades are displayed in Figure 1.3.

Figure 1.4. Horizontal Axis Wind Turbine Rotor Designs: Two blades (a), three blades (b), four blades (c) (LearnEngineering.org, 2013)

The increase of the number of blades results in the increase of the system cost, along with some challenges of the mechanical design of the blades. Therefore, with that in mind and also with

the goal of good efficiency, generally the three bladed wind turbines are used because it can accommodate all the parameters needed for good and efficient system operation.

1.7 Scope of Research

In the present study, six different blade designs are analyzed with wind tunnel testing and numerical simulations. The objective of this thesis, as advised by the research adviser, will be to find a highly efficient HAWT design by conducting a series of studies on the aerodynamic characteristics of the blade shapes. To meet the set objectives, the establishment of 2D and 3D CFD models of wind turbine blades will be required. With that said, a certain number of steps will need to be taken:

(1) Design the models using CAD software, SolidWorks and ANSYS,

(2) Generate numerical mesh around all of the turbine models using Fluent

(3) Create a fluid flow field around the models

(4) From the flow field, determine the drag coefficient and lift coefficient at various wind speeds

(5) Complete some numerical computation to find the power coefficient using torque coefficient.

These designed models include a traditional airfoil and the combination of airfoil to create a blade with high lift coefficient. Wind tunnel experiments are conducted to find power generation and the effect of blade design on the power. Computational Fluid Dynamic (CFD) simulations are performed with ANSYS Fluent to study aerodynamic characteristics of the models. The objectives of the research are as follows:

- Increase power coefficient of horizontal turbines by creating new blade geometries
- Determine the effect of the blade airfoil choice on the power generation

- Design and implement new test fixtures to accompany 3D printed turbines

- Develop a three-dimensional and transient model for HAWT simulation

- Improve the existing subsonic wind tunnel by fabricating a new model test section

If the power production of a turbine is intrinsically dependent on the blade design, then by variating the airfoil types in the design the power generation from the wind turbine should considerably experience an important increase of the overall performance

1.8 Contributions to Scientific Knowledge

The present research provides a certain number of contributions to the horizontal-axis wind turbine body of knowledge. It is important to point out that in the field of wind energy research, not a large number of persons have developed a three-dimensional dynamic analysis using ANSYS Fluent commercial software for the study of HAWTs combining multiple airfoil types in a blade. A detailed approach of the 3D, transient simulation is outlined in this thesis. New blade geometries are tested and compared to standard blades. These models are produced with new 3D printing technology. Recommendations for future work are provided to further improve HAWT performance based on the findings of this research.

1.9 Organization of the Thesis

The present thesis is articulated according to the following steps. A comprehensive literature review of current HAWT technologies is organized in Chapter 2. The review covers drag-based wind turbine technologies. Several papers are reviewed relating to the performance of a horizontal axis wind turbine. Methods for experimentation and numerical analysis are discussed.

The experimental and numerical methodology for completing the research is described in Chapter 3. Design of test setups and equipment for wind tunnel experiments is included as well as

the methodology for the ANSYS Fluent simulations. Additionally, mathematical expressions are provided for calculating wind turbine efficiency, noise effect, and vibration.

The results and analysis of each model tested is covered in Chapter 4. The results will be presented in two sections: experimental and numerical. The findings of this investigation are discussed in terms of power generation, aerodynamic performance, and design optimization.

A summary of the results from this research along with recommendations for future work can be found in Chapter 5. Additional information related to the work, including experimental and numerical data, is available in the appendices.

If the power production of a turbine is directly dependent on the blade design and optimization, then by variating the airfoil types in the design and optimizing the blade design the power generation from the wind turbine should experience a considerably important increase in the overall performance.

CHAPTER 2

LITERATURE REVIEW

2.1 Overview

In recent years, a huge amount of research and resources is being allocated to the sector of energy in the only goal to harness the energy from wind effectively. The main goal in these investigations is to enhance the performances of horizontal axis wind turbines both numerically and experimentally, and the works laid out vary from computational simulations to laboratory measurements on actual models. Improving the conversion efficiency of the horizontal axis wind turbine by manipulating the blades' design to reduce the drag coefficient on the blade, is the primary focus of this entire research. Secondly, it aims to investigate the reduction of noise and vibration effects on the wind turbines overall production in order to increase overall conversion efficiency for realistic wind conditions.

As mentioned earlier, the most important factors that affect the performance of wind turbines are the shape and orientation of the blade cross-section. A microscopic look at the wind turbine blade shows the existence of airfoil cross sections from root to tip. Commonly the driving force of wind turbines is lift force generated when there is a wind flow over a given airfoil. Lift force is always perpendicular to apparent velocity and most of the time lift force increases with the angle of attack. Therefore, the wind turbine will produce maximum performance when the lift and drag ratio is at its maximum. A schematic for lift and drag force induced over a wind turbine blade is provided in figure 2.1.
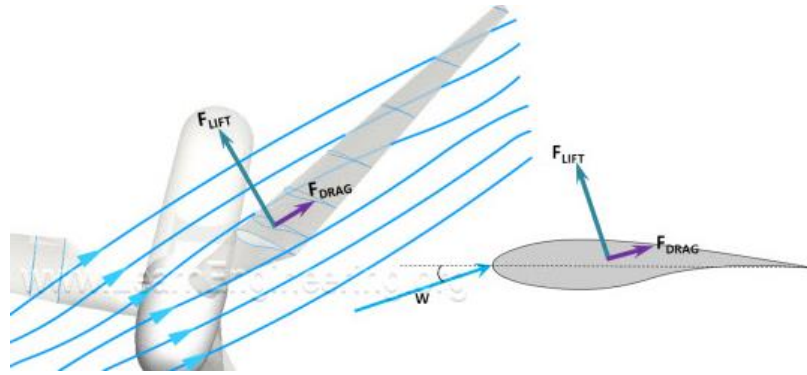
Figure 2.1. Lift and drag force induced over a wind turbine blade (Fluid Mechanics, Wind Power 2013)

2.2 Introduction

With the rising demand for global energy in the past two decades, alternative renewable energy sources are very critical. While it may seem surprising, wind energy is becoming more popular as a renewable source of energy and is justified as a renewable energy source because the wind is an abundant and available resource all year. Many researchers have dedicated their careers in research and development of wind energy systems. It is worth mentioning that there are two main kinds of wind energy conversion systems used. Indeed, the two main types of wind energy conversion systems are the Horizontal Axis Wind Turbine (HAWT) and the Vertical Axis Wind Turbine (VAWT). For several years, HAWTs and VAWTs have been used for large scale power generation. However recently, research on HAWTs has gained more interest. Although HAWTs have many negatives, with some design and performance improvements, it will be more efficient, attractive, durable, and best suited for both small scale and off-the-grid power generation applications. In the following sections, some of the theories of wind turbine aerodynamics and computational fluid dynamics will be discussed. In addition to discussing the purposes and methods of the HAWT stimulation, investigating the computational fluid dynamic analysis of HAWT for optimum power generation will be at the center of our discussion. To achieve the listed

goal of the present study, we have decided to select NACA 0018, NACA 2412, NACA 4412, and NACA 6412 airfoils to conduct the CFD simulations by changing the blade angle as well as the wind speed in order to clearly determine the ideal angle of attack for maximum power generation.

2.3 Airfoil and General Concepts of Aerodynamics

A sectional shape of a horizontal axis wind turbine (HAWT) blade is made of a two-dimensional airfoil, which generates a different force due to the pressure difference across the airfoil. The forces resulting from the airfoil are the lift and drag forces. For design purposes a commonly used theory is adopted, the blade element momentum (BEM). The BEM is used as an outline of the procedure for the aerodynamic design of the HAWT blades. It is worth mentioning that each airfoil has a specific structure with specific geometric shapes that are utilized in order to create a mechanical force, with the contribution of the motion of the airfoil. It is then to affirm that all wind turbines blades use airfoils to generate mechanical power, and the blade cross-section shape is dictated by the airfoils. Each blade has its own characteristics and the width and length of the blade are believed to be the desired function of certain aerodynamic performances, as maximum rotor power and strength are taken into consideration. In order to fully understand all the details on wind turbine investigation, the concepts of an airfoil and aerodynamics need to be clearly outlined.

When the term airfoil is used, it is followed by a certain expression characterizing the airfoil. In the below schematic (figure 2.2) diagram of an airfoil the camber line can be seen, which is the locus of points halfway between the upper and lower surfaces of the airfoil. In addition, there is the chord line which is a straight line attached to the leading and trailing edge. Finally, there is what is called the angle of attack and is defined as the angle between the relative wind and the chord line.
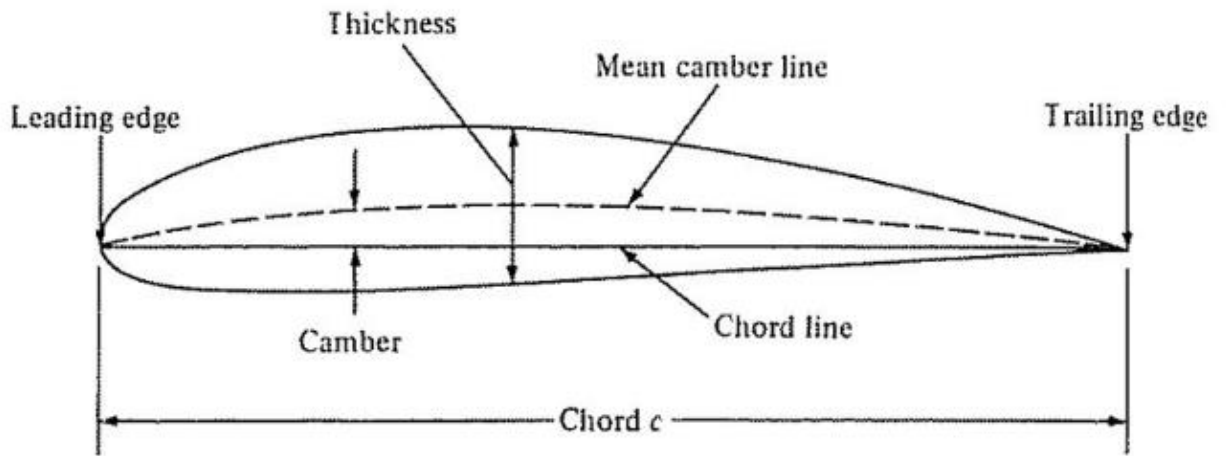
Figure 2.2. Schematic of an airfoil and Nomenclature (James F Marwell, Jon G Mcgowan, and Rogers 2015)
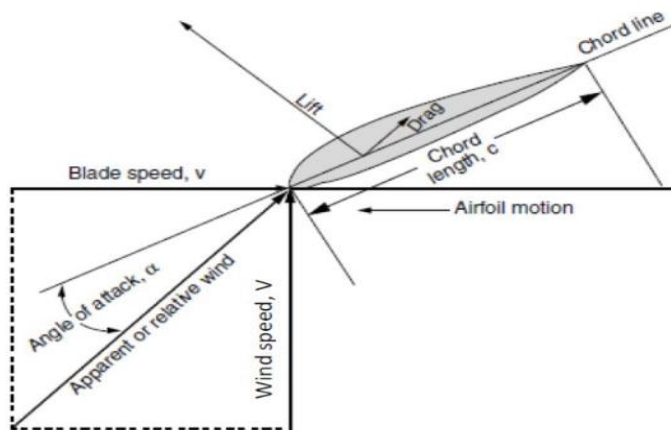
Figure 2.3. Schematic of an airfoil and Nomenclature and characteristics (James F Markwell, Jon G McGowan, and Rogers 2015)

Nowadays, there are so many different types of airfoils used in wind turbines blades, and the one selected and used in the blade designs for the purpose of our investigation is displayed in Figure 2.3. The NACA 0012 is a 12% thick symmetric airfoil. The NACA 2412 similarly is 12% thickness, and according to the Airfoil Tools database a NACA the four digits of the airfoil control four digit. For instance, if an airfoil is NACA MPXX then the first digit (M) represents the

maximum camber divided by 100. In the case of the NACA 4412 M is 4 which indicated 4% of

the chord. The second digit (P) represents the position of the maximum camber divided by 10 and

in the case of the NACA 6412; P is four so the maximum camber is 40% of the chord. According

to the same database, the last two digits represent the airfoil thickness. All the airfoil chosen for

the investigation has the same thickness of 12% of the chord.

Example: NACA 2412

NACA 2 4   12

| Camber in percentage of chord $y_c = 0.02\ C$ | Position of camber in tenths of chord $x_c = 0.4\ C$ | Maximum thickness (t) in percentage of chord (t/c)$_{max}$ = 0.12 |
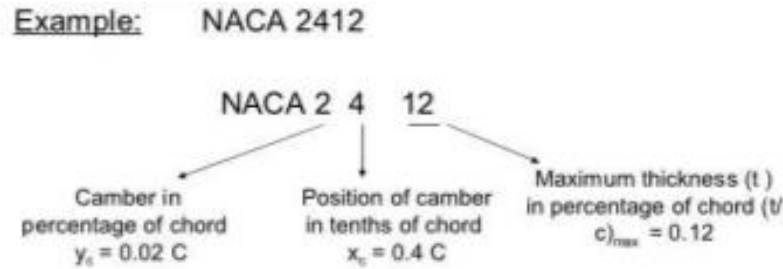
It has been observed that the flow of air over an airfoil is followed by a distribution of

forces over the airfoil surface and the velocity over the airfoils increase over the convex surface,

allowing a lower average pressure to take place on the suction side of the airfoil. The transition

between airflow and pressure distribution drag forces are known because of both pressure

distribution over the airfoil and the friction between the flow of air and the airfoil. The drag caused

by friction is a function of the viscosity of the fluid and dissipates energy into the flow field. The

same airfoils characteristics have been investigated in the Journal of Aerospace Engineering and

Technology by Sanjay N. Havildar and Anklet Rishi, in which their research was to compare the

experimental coefficient of lift and drag for NACA-MPXX. At the end of their investigation, using

NACA 2412, they have concluded that the experimental results indicate a high lift coefficient.
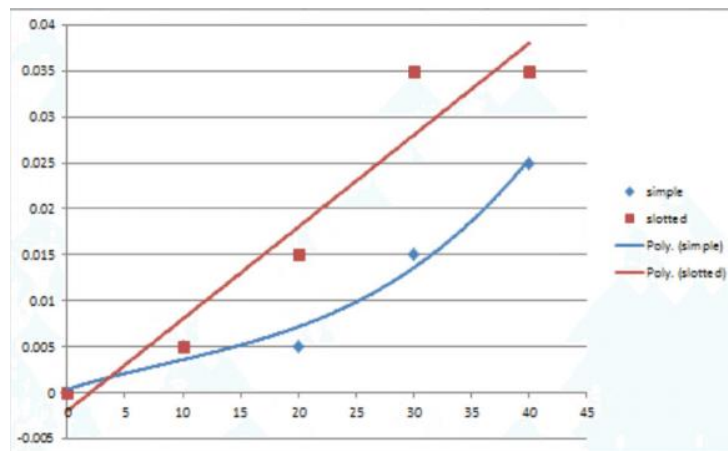
Figure 2.4. Plot of Lift vs Angle of Attack for V= 8ms (STEM Journals, 2015)

2.4. Aerodynamic Analysis of the Horizontal Axis Wind Turbine Blade

In this experiment, an alteration was put on a HAWT blade by using different blade angles in comparison to existing experimental data. Throughout this study, it was proven that the HAWT efficiency is intrinsically related to the blade profile and its orientation (angle of attack). It is possible that the optimum angle at which HAWT generates is at a constant output. To fully understand the objective of the present study, we need to examine more closely the concept behind the lift and drag force and certain aspects of the design. Power is generated via wind speed so that there is a higher lift force and lower drag force. Also about the blade, studying the effect of the angle of attack is a critical aspect that must not be neglected. According to the International Journal of Engineering Research and Application, 'if the angle of attack on the blade is greater than a certain constant value, the mechanism will have to have a small lift force.' Similarly, the smaller the angle of attack, the greater the lifting force and the lower the drag force produced; consequently, this drives more power. In the same perspective, Abhishek Choubey and Bharat Gupta concluded, in their research paper published in the International Journal of Engineering Research and Application (IJERA), that HAWT efficiency depends on the blade profile and blade

orientation. They also found an optimum at which the HAWT operates in optimum condition. On a final note, it is worth noting that the aim of the researcher in this area of aerodynamic analysis of the HAWT is to evaluate the performance of variable-speed fixed-pitch HAWT blades using at least a two-dimensional CFD analysis. The objectives are to analyze the aerodynamic performance of different airfoils, to anticipate the wind turbine power output at different wind speeds, and to predict the noise and vibration of the wind turbine under operation.

2.5 Blades Shape for Ideal and Optimum Rotor

Most turbine blade designs are constituted of 2 or 3 blades rotating around the horizontal axis. Since the blade design is playing a key role in the wind turbine effectiveness, it is normal to wonder what the blade shape should be like. The real question became; which blade shape would produce maximum energy? According to Fei-Bin Hsio and Wen-Tong Chong (2013) in their investigation of the blade geometries, they have discovered that an optimum blade design is obtained by improving the blade element. Their second observation was that an un-tapered and optimum twist blade improves the turbine power production. The researchers went ahead to add that an accurate prediction of a HAWT blade performance depends not only on the blade shapes but also heavily depends on the CFD simulation of a full-scale blade condition. As the previous researchers have utilized the momentum theory and the blade element theory to address the blade shape in the turbine blade performance, J. F. Manwell and A.L. Rogers in their book, Theory, Design, and Application of Wind Energy (2015), explained the implication of both of these

theories in the design process. According to these authors, the blade shape can be approximated so that it will give the maximum power by focusing on the design tip ration for a real wind turbine.

2.6 Changing Number of Blades

An investigation performed by Franz M et al (2016) put an emphasis on the effect of changing the number of blades on a turbine rotation. In their study, a comparison between two and three bladed rotors was performed and it was found that the number of blades is not influencing the velocity deficit in the wake and thus the potential inflow velocities of a downwind turbine can not be neglected. Saha et al. (2008) found that from a structural point of view, the downstream turbine operating in the wake of a 2-bladed turbine experiences higher turbulence levels, which can lead to an increase of fatigue loads in the blades structure.

2.7 Computational Fluid Dynamic (CFD) approaches

CFD simulations combined with experimental studies provide the most informative results for HAWT research. The CFD approach is an inexpensive method for predicting performance prior to fabricating models. In addition, in the previous research, the focus was on the numerical investigation of three blades from the aeroelastic effects on the wind turbine blades. The present work aims to numerically analyze the HAWT rotor and to validate the results of the experimental data. This study focuses mainly on the pressure distribution on the blades, the generated torque, and the general overview of the flow field around the rotor. It is important to note that several CFD methods were focused on isolated rotor cases, but few researchers have studied the effects of the tower on the turbine performance. It should be noted that the research that will be conducted uses an isolated rotor for a 4 blade design and full wind turbine in order to make a true CFD model. The CFD technique proved to be a useful design tool for improving Savonius HAWTs.

Recently, Abdelrahman M.A, and Stanislav (2015) completed a CFD simulation of several HAWT blades. In the simulations they performed, a shear stress transport (SST) k-w turbulence model was necessary using ANSYS Fluent software. The goal of their investigation was to compare the performance of different shapes of the blade. These authors in their researches used two-dimensional and three-dimensional approaches to approximate the Reynolds Averaged Navier-Stokes (RANS) equations. In addition, for accuracy and achievability different CFD approaches for a HAWT investigation were presented. Finally, tetrahedral elements were needed to characterize the mesh, and the solution model was set using the option of the least squares cell-based with second order interpolation. The realizable k-epsilon turbulence model is recommended in the case of a two-equation turbulence model to account for rotation and strain in the flow (Sagol, Reggio and Ilinca 2012). In the case of dynamic simulation, a moving reference frame solution should serve as the initial condition for the sliding mesh calculation (FLUENT Manual 2012).

2.8. CFD Performance Analysis for Horizontal Axis Wind Turbine with Different Blade Shape and Tower Effect.

In this area of research, the focus is on the BEM method, keeping in mind that the HAWT efficiency depends on the blade geometry. The aim of the research done by Janvier Martinez Suarez and Oskar Azul was to determine the best blade shape design. According to the performance test of different horizontal axis wind turbine blade shapes, there are three different HAWT blade geometries. These are the optimum blade (OPT), the un-tapered with an optimum twist, and the un-tapered and untwisted blade. However, according to Fei-Bin Hsio and Wen-Tong Chong (2013) in their investigation of the blade geometries, they concluded that the different experimental results show that the OPT blade is more efficient than the other two types of blade shapes.

2.9. Dynamic Stall

The dynamic stall concept of pitching airfoils has been investigated for many years and several analytical designs were developed to quantify the effects of unsteady loads arising because of the variation of the angle of attack (AOA) of an airfoil. In the wind industry, the dynamic stall has been used to conduct a load analysis in different stages of design. One of the novices of the analytical dynamic stall model was the Boeing-virtual model, investigated by F.J, Tarzanin. Based on Tarzanin's experimentations, a relationship between dynamic stall angle and the static stall has been made by interpolating the load coefficient from the static data. In a similar investigation, C.T. Tran and D. Petit developed another model of airfoil called ONERA. In this newer model, they used a differential equation to fully represent the load coefficient. They describe the load coefficient by the differential equation which is split into two domains. The first order equation is used for a small angle of attack and a stall domain identification, and the second for a high angle of attack region.

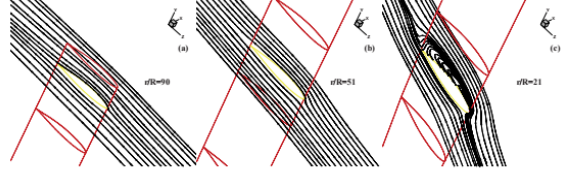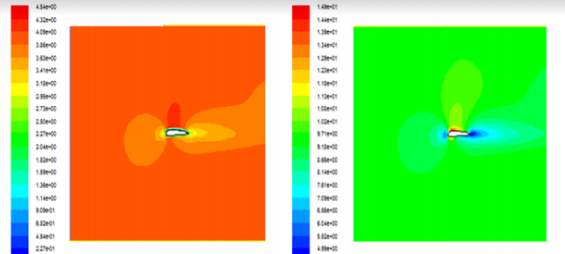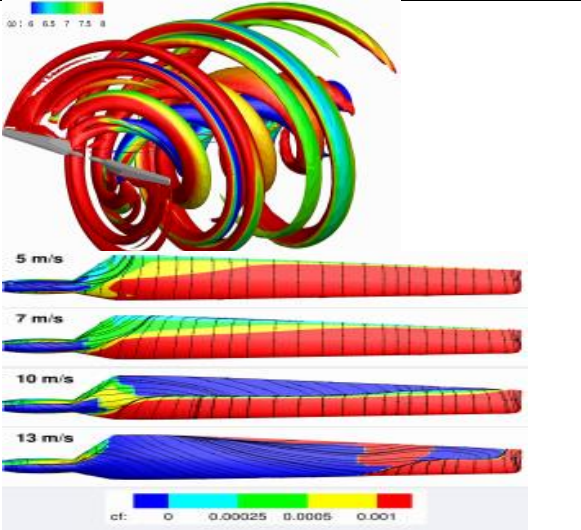## 2.10. Vibration-Induced Aerodynamic Loads

Due to the unavailability of computing resources, computational fluid dynamic techniques have been used to investigate the vibration induced aerodynamic load on HAWT. Xiong Liu and Cheng Lu studied the simulations of unsteady aerodynamic loads on the airfoil, and the incorporation of vibration-induced velocity in acronymic load analysis. The above investigation has permitted researchers to draw a conclusion that the blade vibration has a huge amount of influence on the aerodynamic fatigue loads on the blade of large scale HAWTs. Also, they concluded that for large-scale wind turbines, the effect of the blade vibrations should be considered
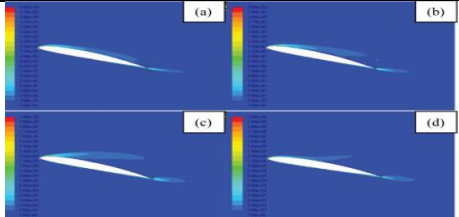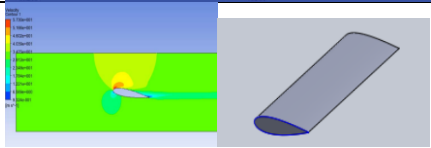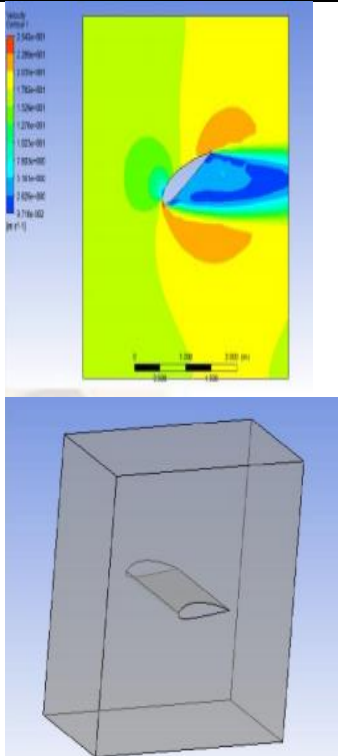
in order to calculate AOA in the acronymic analysis to achieve optimum structural strength and control system design

2.11. Summary of Theoretical Framework

A summary of the theoretical investigation of the present research authors' work and key findings led to the framework of the research presented in this thesis, and is displayed in Table 2.1.

Table 2.1. Summary of HAWT research

Researcher(s)	Studied	Findings	Figure
C.J Bai, F.B. Hsiao and Y.J. chen(2015)	Design of HAWT Blade and Aerodynamic Investigation Using Numerical Simulation	Simulation results indicate that CFD is a good method on aerodynamic investigation of HAWT blades	 Fig. 7 The streamline plots at r/R=90 %, r/R=51 % and r/R=21 %.
Ngala, G.M., Shuwa, M., Oumarou, M.B. and Muhammad, A.B. (2015)	CFD Analysis Of a macro Horizontal Axis wind turbine Blade	maximum of 142.66 watts was extracted with a wind speed of 3.89 and at a angle of 8 degree	
Javier M. Suarez and Oskar szulc (2015)	Prediction of aerodynamic characteristics on HAWT	the stall initialization occur with the increase in wind speed in modern wind turbine rotors	

B. Raeisi and H. Alighanbari (2014)	CFD Analysis of Oscillating Blades for Small HAWT in Dynamic Stall	Ansys-fluent is a powerful tool in the investigation of dynamic behavior of a oscillating airfoil in unsteady condition	
Monir Chandrala, Abhishek Choubey, Bharat Gupta (2013)	CFD Analysis of HAWT blade for optimum power	The investigation has shown that the blade at a minimum angle of 10 degree offer optimum power.	
Monir Chandrala, Abhishek Choubey and Bharat Gupta (2012)	Aerodynamic Analysis of HAWT Blade	HAWT efficiency is highly depends on the optimum angle at which the HAWT gives constant output. A constant power is obtained between blade angle 22.5 to 60 degree	

2.12. Motivation for Research

According to the above literature review, some unexplored areas in the HAWT research are identified. First, only traditional geometries are used for designing the blades. Second, there is no available data for blade design combining different airfoil types, even though positive results are seen with airfoil twist angles in low TSR ranges. Also, there are plenty of research involving changing the number of blades for standard turbine blades, but none for noise and vibration by the

models. Finally, very few researchers have developed three-dimensional and transient flow simulations for the study of aerodynamic behavior of wind turbines with a winglet. With these in mind, the following points are outlined for the thesis:

- Improve the existing subsonic wind tunnel by developing a new data acquisition system for HAWT model test section

- Modeled the blade geometries in SolidWorks using different airfoil geometries

- Validate any possible increase of performance of the new designs with a numerical simulations

- Make 3D prints of all models for an experimental testing

- Design and implement a new test fixtures to accompany the 3D printed turbines

- Investigate the performance of each model using ANSYS Fluent simulation and plot the power coefficient vs. tip-speed ratio

CHAPTER 3

METHODOLOGY

3.1 Introduction

In this section, the procedures for the experimental and numerical studies will be covered. The majority of the experiments in this research are tested with an open-type subsonic wind tunnel. At each wind speed tested, the power generated, the wind velocity, and the energy data are collected. The use of a Labquest software is introduced for the experimental portion of the research. ANSYS Fluent software is also used for the computational fluid dynamics simulations. The simulations are performed in the main objective to compile computational data over time for three blade turbines.

3.2 Models Design and Fabrication

In total, four HAWT models are tested in the present investigation. SolidWorks is used to develop each model. Because of the complexity of some blade geometries, all the models are 3D printed using fused deposition modeling (FDM) and stereolithographic (SLA) methods. The models are named SA-NACA 0012, SA-NACA 2412, SA-NACA 4412, SA-NACA 6412 and CA-NACA 00-24-44-64 for reference. The traditional HAWT Blade model is used to compare the results of the new designs. The CAD model of each blade's design and a brief description, as well as the traditional blade, can be seen in the figures below.

Revision 1
Brief Description: First revision of the original airfoil. A redesign was needed, especially at the root that experienced a failure at un-filleted intersection between the base and the root.
Blade Design: NACA 0021, angle of twist 20.0° within tapered airfoil. The NACA0021 design was used because of its symmetrical properties about its chord line.

Root Design: Simple extrusion of the radial circle into the cylindrical root fixture. An angle made between base and root due to extrusion.

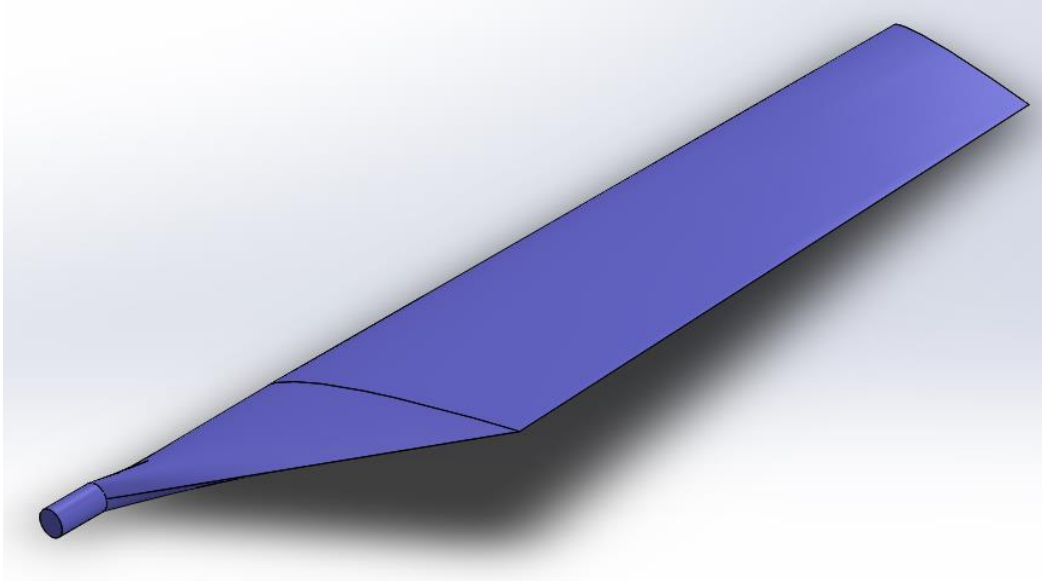**Results:** Failure at un-filleted intersection between the root and the base due to a stress concentration at union.

Figure 3.1. First Blade Design Using NACA 0021

Revision 2

Brief Description: Based on the structural results tested in ANSYS, a redesign was much needed to avoid drastic results as seen in revision 1

Blade Design: The base to tip ratio was readjusted in order to make the base a more tapered look. Also we added the following airfoils NACA (0012, 2412, 4412, and 6412). The airfoils chosen were picked specifically because, all of them have a common 12% thickness. From there the idea of having the most drag at the base and the most lift at the tip was the key aspect in choosing the airfoil with an increasing camper to increase its overall lift force. The angle of twist was 20° from the base airfoil (NACA 0012) to the tip profile (NACA 6412)

Root Design: The root design for revision 2 came after the structural failure from revision 1 in order to readjust the design so that it would fit flush with the hub. The downside to this design was the limited angle of attack that was available.

Results: This blade did not break, we had a successful redesign attempt.
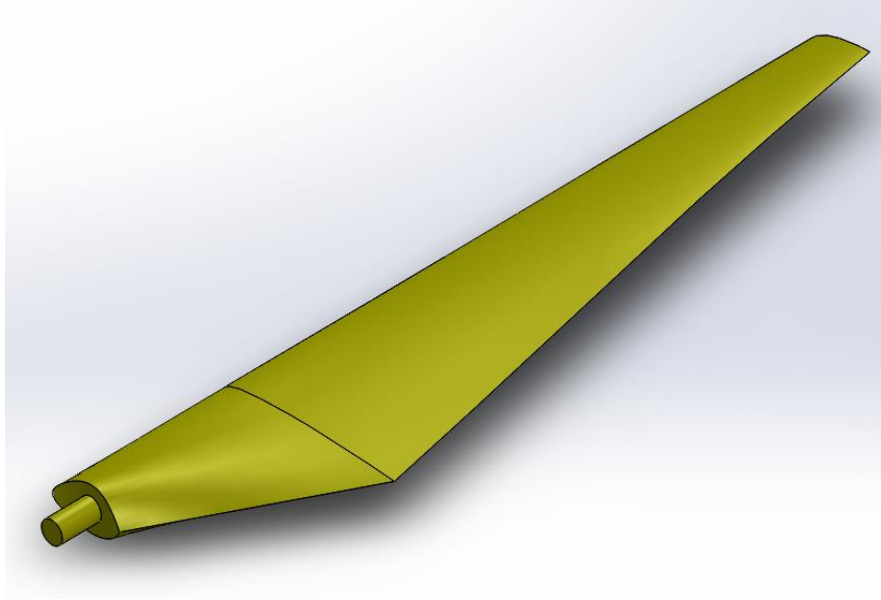
Figure 3.2. Second Blade Design Using NACA 6412

<u>Revision 3</u>

Brief Description: Based on the previous experience, the blade was redesigned for a thicker base and also to be able to generate a higher power output.

Blade Design: The blade was redesigned with a combination of 4 different airfoils. The angle of twist was readjusted to 15 degrees. The base to tip started from NACA 0018 >> NACA 2412 >> NACA 4412 >> NACA 6412. The NACA0018 profile replaced the NACA 0012 profile in revision 2 because the NACA0012 was too thin and the loft feature in SolidWorks would not work until we changed it to NACA0018, which is a 6% increase in the overall thickness.

Root Design: The root was redesigned to reduce the stress concentration and relocated it straight along the leading edge.

Results: The root experienced failure at 5 m/s due to the stress concentration between the root and the base. The blade (No tape) generated 117 mW at 5.15 m/s, and the highest efficiency is 3.6% occurring at 2.6 m/s. The power output of the blade slightly increased with the tape added on the blade. The efficiency increased up to 4.8% at 3.1m/s
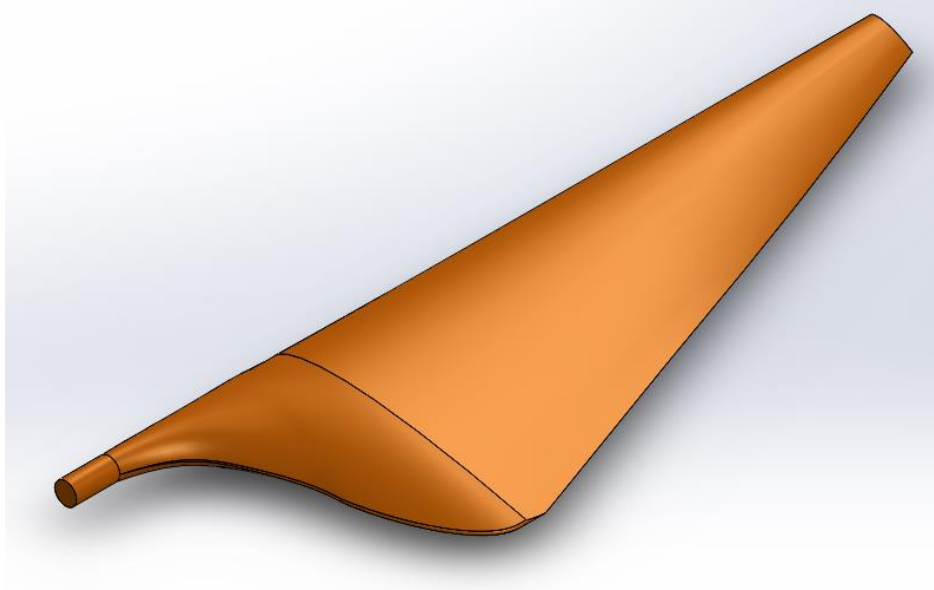
Figure 3.3. Third blade design using NACA 0018

Revision 4

Brief Description: Better base design.

Blade Design: The same airfoils were used in revision 3, but the length of the blade increased by 1 inch and the taper of the blade decreased. The chord length of the tip is now 0.25 inch longer.

Root Design: The distance from the NACA6412 profile to the root was decreased by 1 inch to decrease the stress concentration.

Results: A maximum of 24.37% efficiency was calculated at a wind speed of 2.5 m/s.

Figure 3.4. Fourth Blade Design Using NACA 6412

Revision 5

Brief Description: Better base design.

Blade Design: The same airfoils were used as in revision 2, 3 and 4, but the length of the blade increased by 1 inch. The taper of the blade decreased and the chord length of the tip remained 0.25 inch longer.

Root Design: The distance from the NACA 1412 profile to the root decreased by 1 inch to decrease the stress concentration.

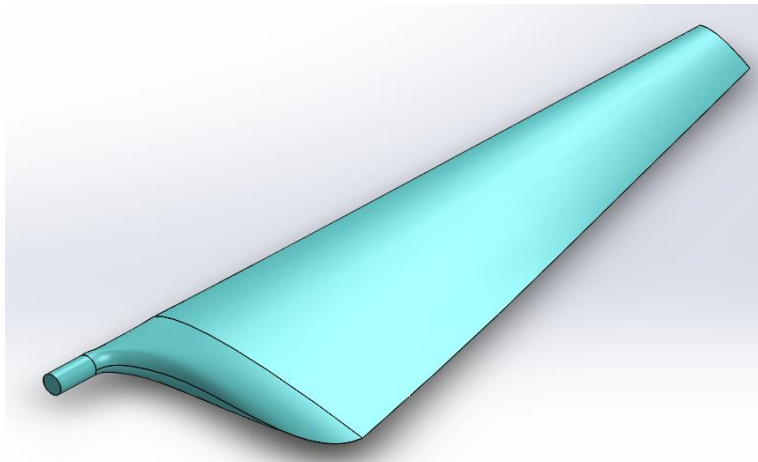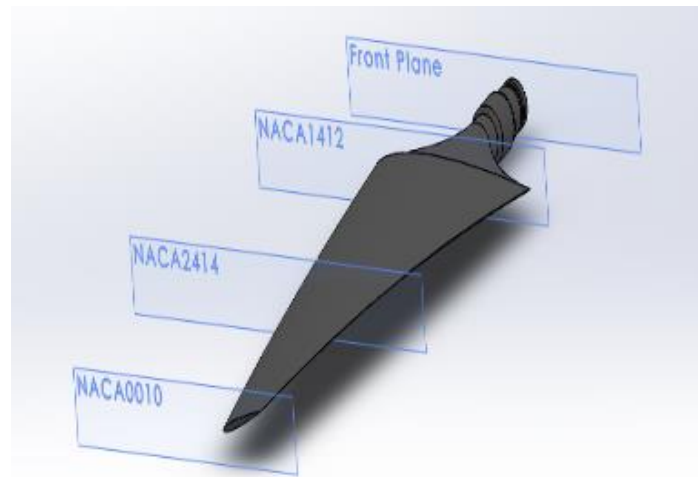**Results:** A maximum of 24.37% efficiency was calculated at a wind speed of 4 m/s.

Figure 3.5. Fifth Blade Design Using Mix NACA Airfoils
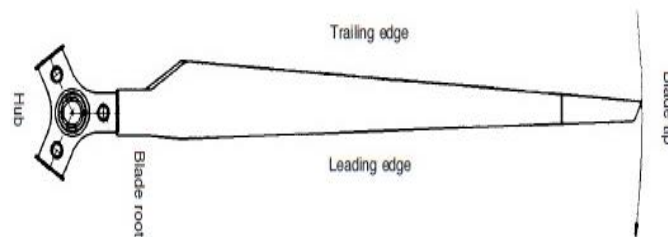

Figure 3.6. HAWT Traditional Blade

In this study, each individual model is designed with a 10-inch blade radius (R) and a 4-inch blade root (W); therefore, the swept area (A) was consistent across all models. A typical HAWT blade and region classification is displayed in figure 3.7.

Chord length (C_{opt})

Radius (r)

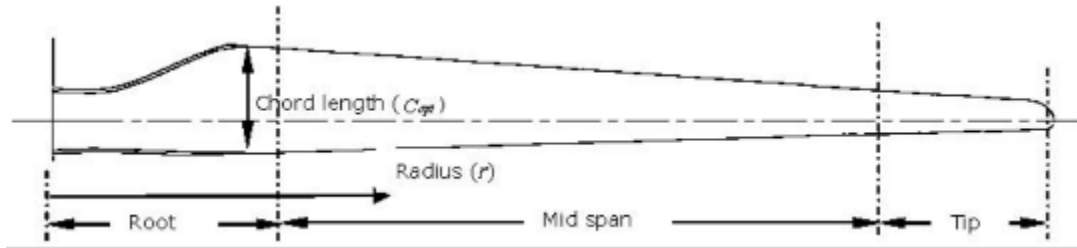Root   Mid span   Tip

Figure 3.7. Typical HAWT Blade Plan and Region Classification. (Peter J. Schubel and Richard J. C)

Throughout the process of the blade's optimization method, a particular emphasis is primarily on the blade plan and design tip speed ratio. It is helpful to reduce the area of the solidity of the blade tip speed ratio as it leads to a decrease in material usage and manufacturing cost reduction. Presented in figure 3.7 and 3.8 are the blade plan shapes for alternate design tip speed ratios.
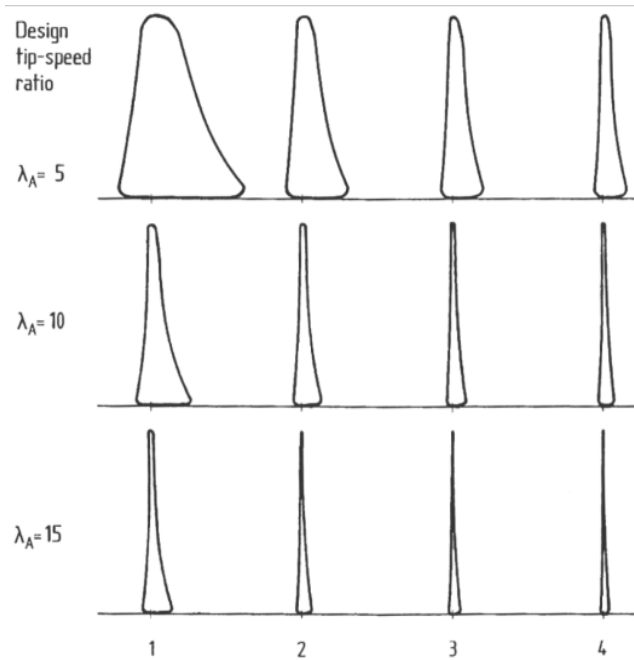
Figure 3.8. Blade Plan Shape for Alternate Design Tip Speed Ratios.

The HAWT models in the study are designed with the manufacturing facilitation and the research of optimum chord dimensioning in mind. With what has been mentioned above, it can be concluded that for optimization purposes, the chord dimensioning and the number of blades is negligible in terms of efficiency. The details of the efficiency theory related to losses due to the simplification of the chord length can be seen in figure 3.9. The CAD physical models are created from ABS (PLA) plastic with a FDM 3D printer for the experimental testing.
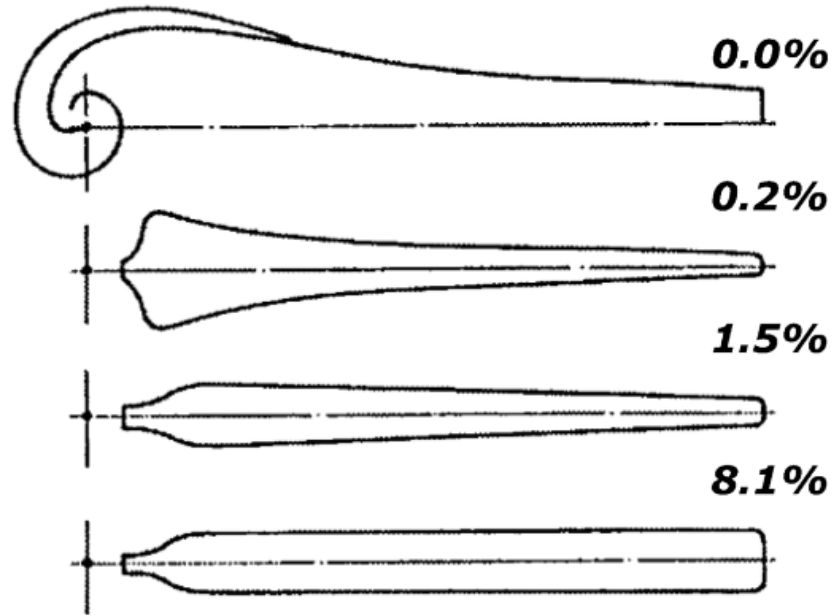
Figure 3.9. Efficiency Losses as a Result of Simplification to Ideal Chord Length

3.3 Experimental Setup and Equipment

The Georgia Southern wind energy laboratory is equipped with a subsonic open-type wind tunnel for experimental testing. The wind tunnel and test section are shown in figure 3.10. The wind tunnel presents two openings, an inlet shown in the far left of figure 3.11 followed by a honeycomb section to generate a laminar flow. A variable frequency drive controls the fan. Another honeycomb section immediately follows the fan. As can be seen in figure 3.11, there is a diverging-converging section with a 9 to 1 area ratio to the 2 ft. by 2 ft. wind tunnel outlet. A VAWT and HAWT test section frame can been seen in figure 3.10. As part of the wind energy research, a new test section is developed for future HAWT and VAWT experiments.

Figure 3.10. Wind Tunnel Configuration for HAWT and VAWT Testing
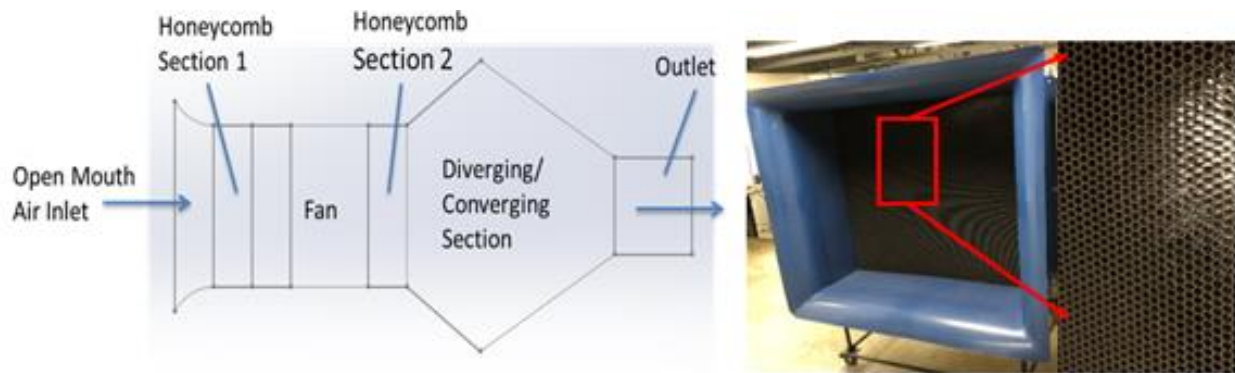
Figure 3.11. Wind Tunnel Sections Schematic

3.4 New Testing Section Design

In order to conduct multiple experiments using HAWT or VAWT models in a lab setting using the wind tunnel, a new testing section is designed and fabricated. Detailed steps and fabrication procedures for the testing section can be viewed in Appendix A. The new testing section as intended by Zongo Relwinde (graduate student) is capable of testing prototype models of HAWTs and VAWTs. The completed assembly is shown in figure 3.12.
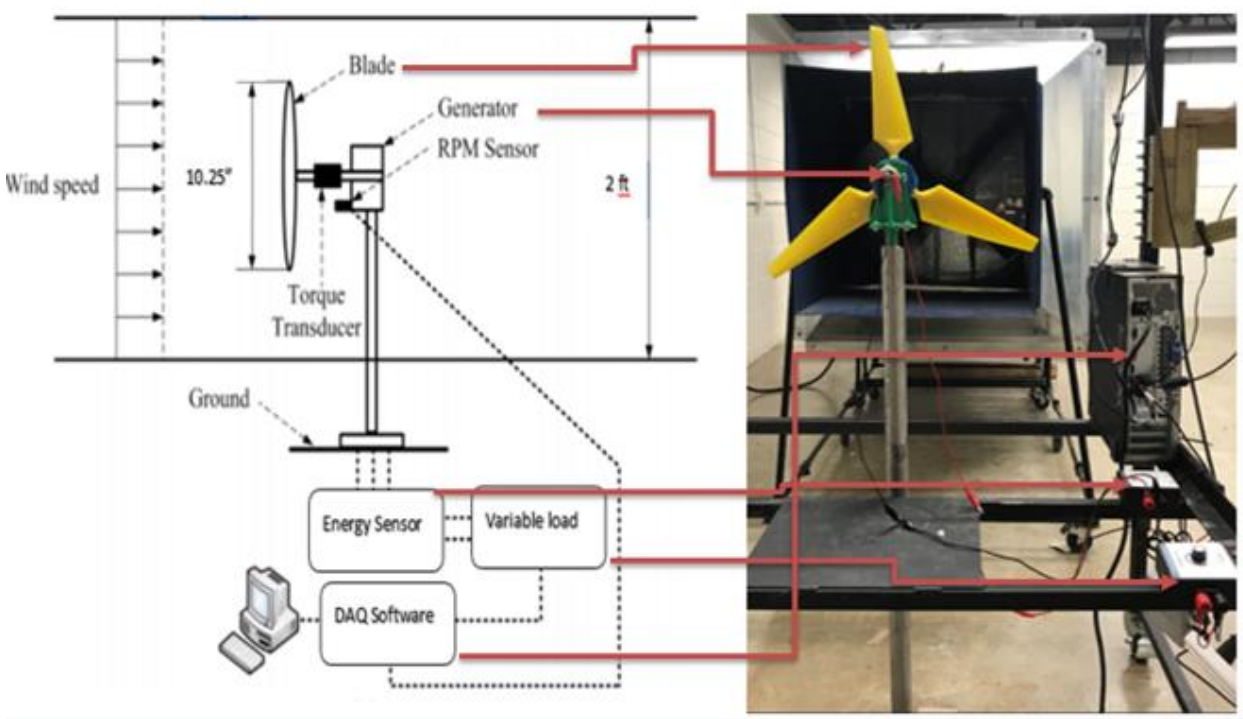
Figure 3.12. Completed assembly of new wind tunnel test section apparatus

3.5 Wind Velocity

A free stream velocity coming from the wind tunnel is conveniently controlled with the variable frequency drive (VFD) operator interface shown in figure 3.13. Consistent and maintainable RPMs of the motor depend on the frequency, which is measured and displayed in Hertz, transmitted from the VFD. The internal fan then produces wind speeds capable of varying from 0 to 20 m/s through the outlet.

Figure 3.13. Huanyang Variable Frequency Drive Operator Interface

3.6 Numerical Procedure and Computational Methods

It is important to mention at the beginning of the computational method that for the study of HAWT, a specific methodology had to be adopted. The mentioned methodology includes the design portion, the calculation, and the computational fluid dynamics. It is also important to note that the first element in the CFD analysis focuses mainly on guided steps. These steps include preparation of the geometry, choosing the type of airfoil to be used, identifying the selection (which is done by calculation) and the meshing and boundary condition portion.

As previously mentioned, the HAWT blade can be designed via the blade element momentum (BEM) technique. Based on the theory of BEM, the blade can be divided into multiple elements. A separate calculation method must be conducted to determine the force and the momentum of the airflow. Firstly, we consider some parameters such as the chord length, blade radial length, the blade relative angle, the blade span, the lift, and drag forces. We decided to

choose a specific profile (airfoil NACA 0012) for modeling using SolidWorks software and the CFD analysis, which will be performed in ANSYS fluent (version 18.1).

The lift force is the force acting on the blade perpendicular to the undisturbed wind flow while the drag force acts on the blade in the direction of the undisturbed wind flow (Kevadiya and Vaidya, 2013). M. Chandra and A. Choubey concluded that the lift force should be high and the drag force should be low; therefore, the goal is to obtain a minimum angle of attack so that the lift force is high and drag force will drop as low as possible. In conclusion, there is more evidence to support that the angle of attack of the wind on the blade has a very important impact on the analysis.

$$F_L \quad = \quad \frac{1}{2} \, C_L \rho v^2 A \quad (1)$$

$$F_D \quad = \quad \frac{1}{2} \, C_D \rho v^2 A \quad (2)$$

The computational fluid dynamic (CFD) analysis using the designed blade is to be carried out to investigate the viability of the blade. To achieve the goals of the investigation, a 2-dimensional geometry of the designed blade must be created within the computational domain. And in the same process of designing a HAWT, we must consider the power generation mechanism. In order to understand how power is generated from wind speed, the following equation can be used:

$$C_p = \frac{P_{rotor}}{\frac{1}{2}\rho A V^3} \qquad (3)$$

Where

P= Power of the wind in Watts

ρ= Air density in kg/m

A= area of a segment of the wind being considered

V = undistributed wind speed in m/s.

The CFD analysis procedure starts by creating a model of HAWT and then the model is saved in IGES files format and imported into ANSYS. The geometry is then generated followed by the meshing. It is important in the meshing process to check the mesh skewness and orthogonal quality, which can be found under mesh detail. The below table can be used as a general guideline to check the quality of the mesh depending on the physical solver used.

Skewness:

Outstanding	Very Good	Good	Sufficient	Bad	Inappropriate
0-0.25	0.25-0.50	0.50-0.80	0.80-0.95	0.95-0.98	0.98-1.00

Orthogonal quality:

Inappropriate	Bad	Sufficient	Good	Very Good	Outstanding
0-0.001	0.001-0.15	0.15-0.20	0.20-0.70	0.70-0.95	0.95-1.00

After the meshing is completed, the next step is the physics setup. Before proceeding in the fluent launcher, the double precision, parallel and number of cores must be selected. Then in models, under edit viscous, select K-omega and SST. Also, in cell zone conditions, under edit fluid, select the frame motion and then specify the velocity. The boundary condition of all parameters must be defined. In the process of defining the boundary conditions, the inlet velocity was set to have a wind speed of 12 m/s and the turbulence ratio was estimated to be 10. In addition, the assumption was made that at the wall there is no-slip condition and the flow discharge at the outlet is done with an assumption that the opening pressure is equivalent to atmospheric pressure. The next step is the numerical solution. In this numerical solution domain, under solution methods, schemes must be changed to coupled, the gradient must be changed to least squares based and the pressure must be changed to standard. Also, the pseudo transient must be selected with high order

relaxation and set the rest of the checkpoints to a second order. The below table can be used as a reference. A complementary element must be added to the boundary condition set up so that the domain type can be set as a fluid domain. The fluid type was selected using air ideal gas and the recommendation was a turbulent flow with an operating pressure of zero. The domain motion is set up as stationary with a heat transfer model as the total energy by selecting the k-epsilon model for the turbulence model.

Domain	Fluid Domain
Fluid	Air Ideal Gas
Domain Motion	Stationary
Heat Transfer Model	Total Energy
Turbulence Model	k-epsilon

After further investigation, we found out that the lift coefficient (C_L) and the drag coefficient (C_D) values can be deduced from the design airfoil workshop for different angle of attack. For example:

10 degrees:

C_L= 1.279.

C_D=0.0144.

A smart fine mesh must be exported to fluent and then applied to the fundamental laws of mechanics of fluids. The equation of conservation of mass and momentum are analyzed and solved based on the CFD Navier-Stokes system equation that is written as follows:

$$\nabla (\rho v) = 0 \qquad (4)$$

At a steady state, the continuity system equation is simplified as

$$\nabla (\rho v) = 0 \qquad (5)$$

In the same way, the flow considered being incompressible, the equation can be written as

$$\nabla (\rho v) = 0 \qquad (6)$$

An example mesh is displayed in figure 3.14. A top view of wireframe mesh is shown on the left, and a sectional view displaying the two separate cell zones is on the right.
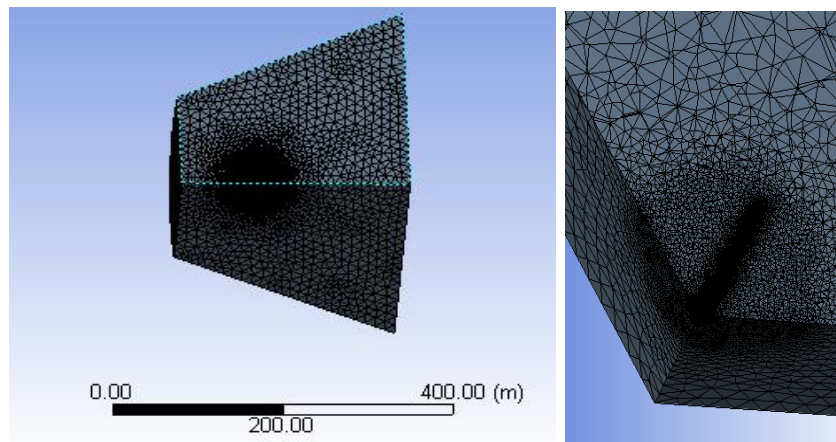

Figure 3.14. Top View of Model Mesh (left) and Sectional View (right)

3.7 Validation and Verification

Before anything else it very critical to take note that the emphasis will be on two verifications to check if the simulation correctly solved the model. In other words, the previously

mentioned step is to ensure that the mass is balanced and the pressure on the blade model has converged.

3.8 Check Iterations

The check of iterations is another essential step to verify whether there is a sufficient number of iterations performed in the process of obtaining the solution (convergence). Indeed, it is critical to check out the solution behavior after a certain number of iterations. In figure 3.14 below, as it is shown after 3,000 iterations the graphs do not show any major variations. The choice of 1,500 iterations was estimated to be appropriate for the present computation due to a solving time reduction. Base on the obtained graphs, it is worth mentioning that the solution seems to be convergent beyond the 3,000 iterations.

3.9 Check Mesh Refinement

In this study, it is very important to take a close look at the mesh refinement because a finer mesh can help achieve a more precise solution of the model. The below figure demonstrates how the results change with a greater number of cells. In this wind turbine blade computational fluid dynamics, the mesh created has around 350,000 cells, which clearly is an indication that the mesh is not fine enough for a very accurate solution. With a goal of refining the mesh to a maximum, some adjustment in global and local mesh controls were taken (relevance center, face sizing, inflation and sphere of influence). It is then that we obtained a mesh of 8 million elements, which is shown in the data plot at the rightmost point. The relevance center was set to 0.05 m, the number of layers increased to 10 at a growth rate of 1.2 and the element size set to 1 m.

3.10 Compare Blade Tip Velocities

In the CFD-Post, the blade tip velocity approached 98.05 m/s and if we compare this value to the hand calculation the results are very close. The hand calculation yields a blade tip velocity of 98.12m/s. In a pre-analysis conducted in the process of the selection of the blade, a prediction of 0.3 of the power coefficient was made. Indeed, in the convergence figure below, the numerical results confirm the prediction if we consider a sufficient number of elements in the mesh. For instance, if a mesh of 2 million cells is used, the power coefficient will be around 38% as opposed to 30% from hand calculations. One thing to keep in mind is that the power coefficient must lie under the Betz limit of 16/27 for a non-shrouded rotor. In this way, it is clear that our numerical results fall below the Betz limit.

3.11 Validation

Currently, with the new testing section developed in the wind energy lab, experimental data is being collected to validate the results. Parallel to the experimental data, a hand-calculation of the expected results can be used for validation purposes. The rated power of the turbine is to be 1.5MW with a rated wind speed of 11.5 m/s and a rotor diameter of 82.5m. The obtained power coefficient (Cp) confirms the power coefficient found from the simulation.

Hand calculations	Ansys	% different
1576.3 KN	1578.1 KN	0.1

In a similar process and by changing the velocity parameter, we were able to obtain PR values that closely match the ones produced by ANSYS as shown below with the hand calculations and different velocity values.

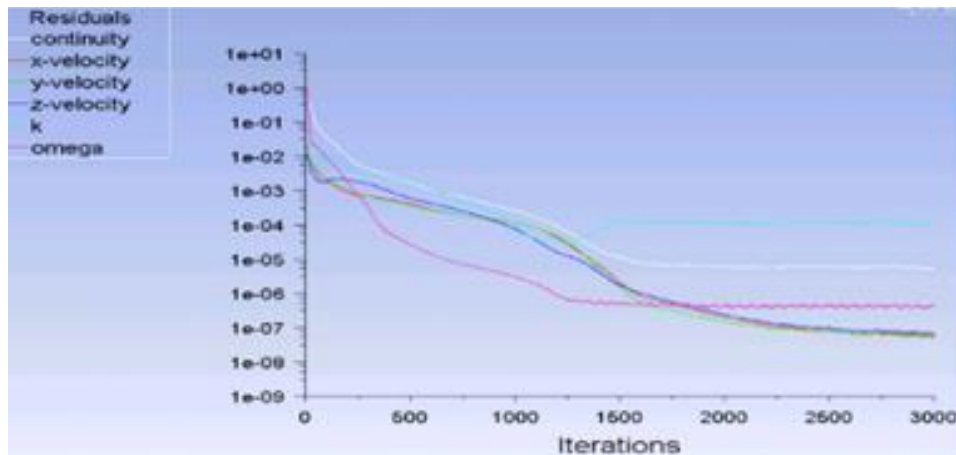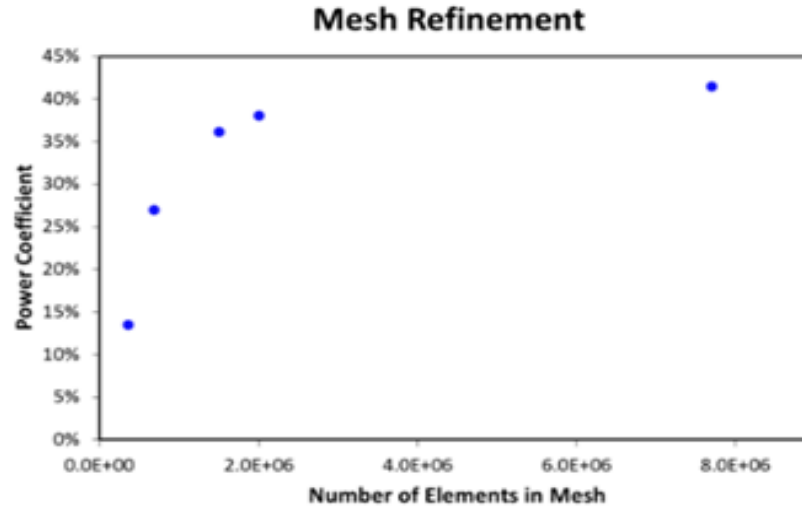| r	44.2	44.2	44.2	44.2	44.2	44.2
w	2.22	5	10	15	22	50
w2	4.9284	25	100	225	484	2500
v	98.124	221	442	663	972.4	2210
pr	1575.847	7993.703	31974.81	71943.32	154758.1	799370.3

Figure 3.14. MRF Residuals Converged After 1500 Iterations and SMM Residuals

3.12 Check Mesh Refinement

In this study, it is very important to take a close look at the mesh refinement because a finer mesh can help achieve a more precise solution of the model. The below figure demonstrates how the results change with a greater number of cells. In this wind turbine blade computational fluid dynamic, the mesh created has around 350,000 cells, which clearly is an indication that the mesh is not fine enough for a very accurate solution.

Mesh Refinement

With a goal of refining the mesh to a maximum, some adjustment in global and local mesh controls were taken (relevance center, face sizing, inflation and sphere of influence). It is then that we obtained a mesh of 8 million elements, which is shown in the data plot at the rightmost point. The relevance center was set to 0.05m, the number of layers increased to 10 at a growth rate of 1.2 and the element size set to 1 m.

Boundary conditions for the simulations are taken from experimental data. These include air velocity, inlet speed and corresponding rotational speed of the blades. The pressure outlet is kept at constant atmospheric pressure. The blade walls are given a no-slip condition and zero rotational velocity relative to the sliding mesh zone (equal to the rotating fluid domain).

CHAPTER 4

FINDINGS OF THE STUDY

4.1 Introduction

In the present chapter, we will cover the results and discussion of all numerical and experimental analyses carried out in the research. The information is organized as followed:

● The first simulation carried out is the structural analyses with different material and loading condition in all four models investigated.

● The next simulation is the computation fluid dynamic testing using 2D airfoils and 3D models blades.

● The 3D Numerical simulations with input boundary conditions from experimental data are completed. The power produced is recorded for each simulation and used for determining the efficiency of each turbine. Each result is discussed and compared to the wind tunnel experiments.

4.2 Blade Models Preparation
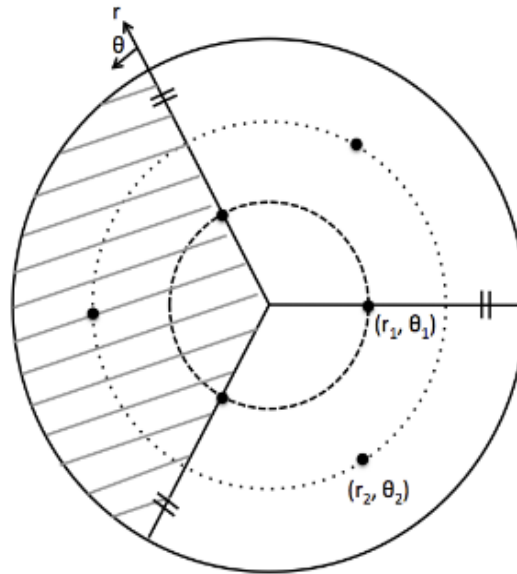
Figure 4.1. Geometry of ⅓ if the Full Domain Periodic Assumption.

The boundary condition of the blade fluid domain is as follows:

1. Inlet velocity 12 m/s

2. Outlet pressure 1 atm
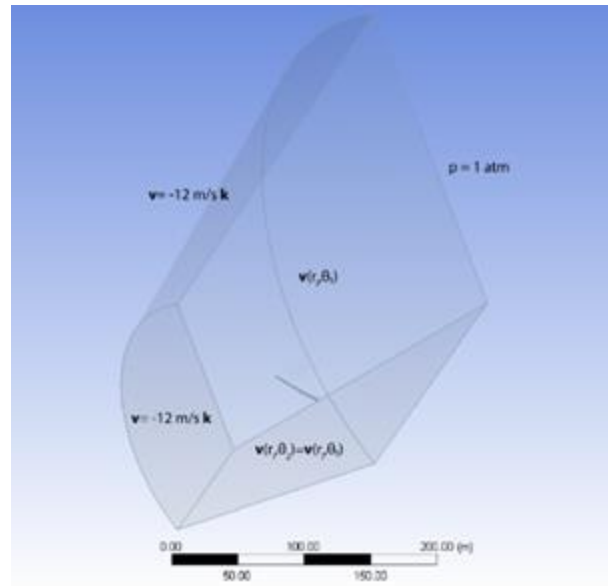
3. Blade: no-slip

4. Side boundaries: periodic

Figure 4.2. Geometry of ⅓ if the Full Domain Periodic Assumption with Boundary Condition.

**Table 4.1. Blades Static Structural Analysis Parameters for Material Analysis.**

		ABS Plastic		Aluminum Alloy		Stainless Steel	
		Medium Mesh	Fine Mesh	Medium Mesh	Fine Mesh	Medium Mesh	Fine Mesh
NACA0010 Air Foil	Total Deformation (m)	6.40E-04	6.40E-04	3.42E-05	3.38E-05	3.55E-05	3.48E-05
	Max Pricipal Stress (Pa)	3.99E+06	3.94E+06	1.00E+07	9.75E+06	2.84E+07	2.74E+07
	Min Principal Stress (Pa)	1.00E+06	1.00E+06	2.98E+06	2.52E+06	9.17E+06	7.89E+06
	Equivalent Stress (Pa)	3.17E+06	3.12E+06	7.96E+06	7.67E+06	2.18E+07	2.13E+07
NACA2412 Air Foil	Total Deformation (m)	6.94E-04	7.04E-04	4.30E-05	4.32E-05	3.67E-05	3.68E-05
	Max Pricipal Stress (Pa)	1.76E+06	1.89E+06	3.88E+06	5.02E+06	1.04E+07	1.47E+07
	Min Principal Stress (Pa)	3.00E+05	3.78E+05	3.85E+05	9.35E+05	2.24E+06	2.46E+06
	Equivalent Stress (Pa)	1.55E+06	2.09E+06	3.44E+06	4.66E+06	9.49E+06	1.28E+07
NACA6412 Air Foil	Total Deformation (m)	1.05E-02	1.03E-02	5.03E-05	5.53E-05	3.44E-07	58546
	Max Pricipal Stress (Pa)	3.87E+06	5.47E+06	8.51E+06	8.02E+06	2.59E+07	6.23E+07
	Min Principal Stress (Pa)	8.66E+05	1.06E+06	3.14E+06	2.07E+06	7.11E+06	1.29E+07
	Equivalent Stress (Pa)	2.77E+06	5.81E+06	6.55E+06	1.38E+07	2.79E+07	4.69E+07

In the blade design process, it was critical to consider the material behavior and understand its importance for the investigation as the research moves to the blade structural analysis. Indeed, the above table was generated using ANSYS FEA, in order to clearly understand the material

behavior of the three potential materials that is being considered for the fabrication of prototype blades.

Table 4.2. Blades Static Structural Analysis.

	NACA 0012	NACA 2412	Ass. Blades
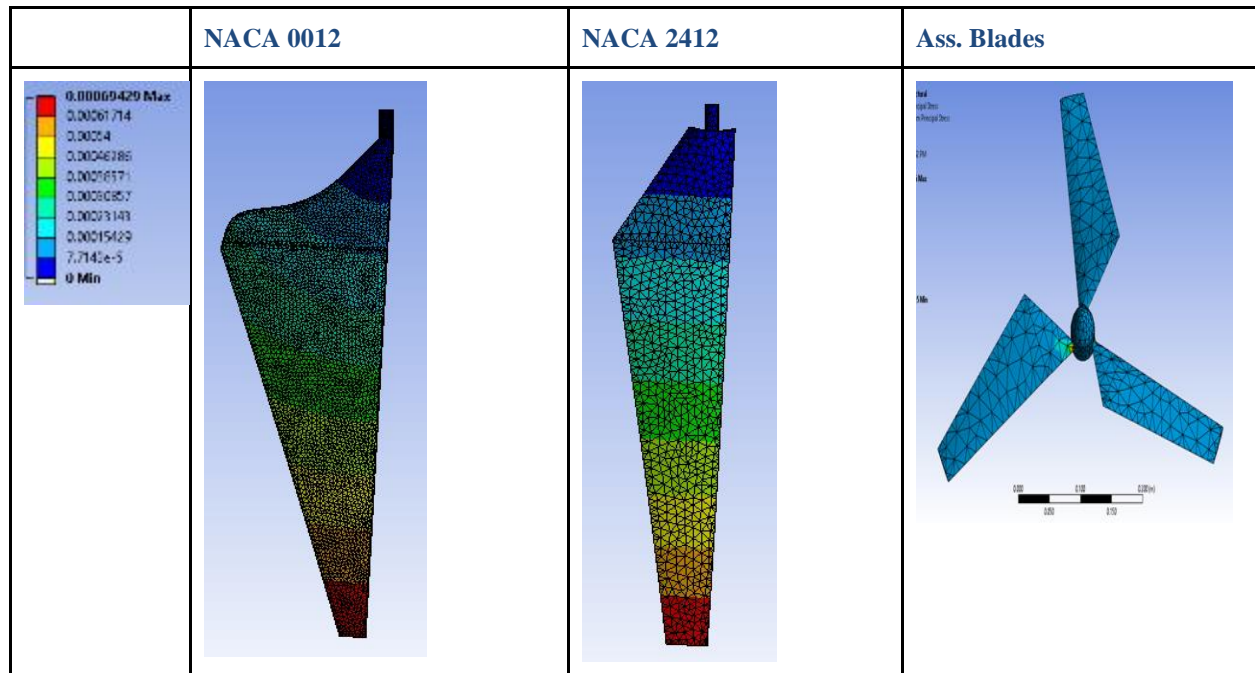
The structural analysis is one of the most important factors in any design, for the simple fact that it allows the analysis to directly comprehend the design structural integrity and strength of the structure. Evaluating whether the investigated blades will be able to withstand external and internal stress and forces expected in the design is as beneficial as determining the cause of failure in the design.
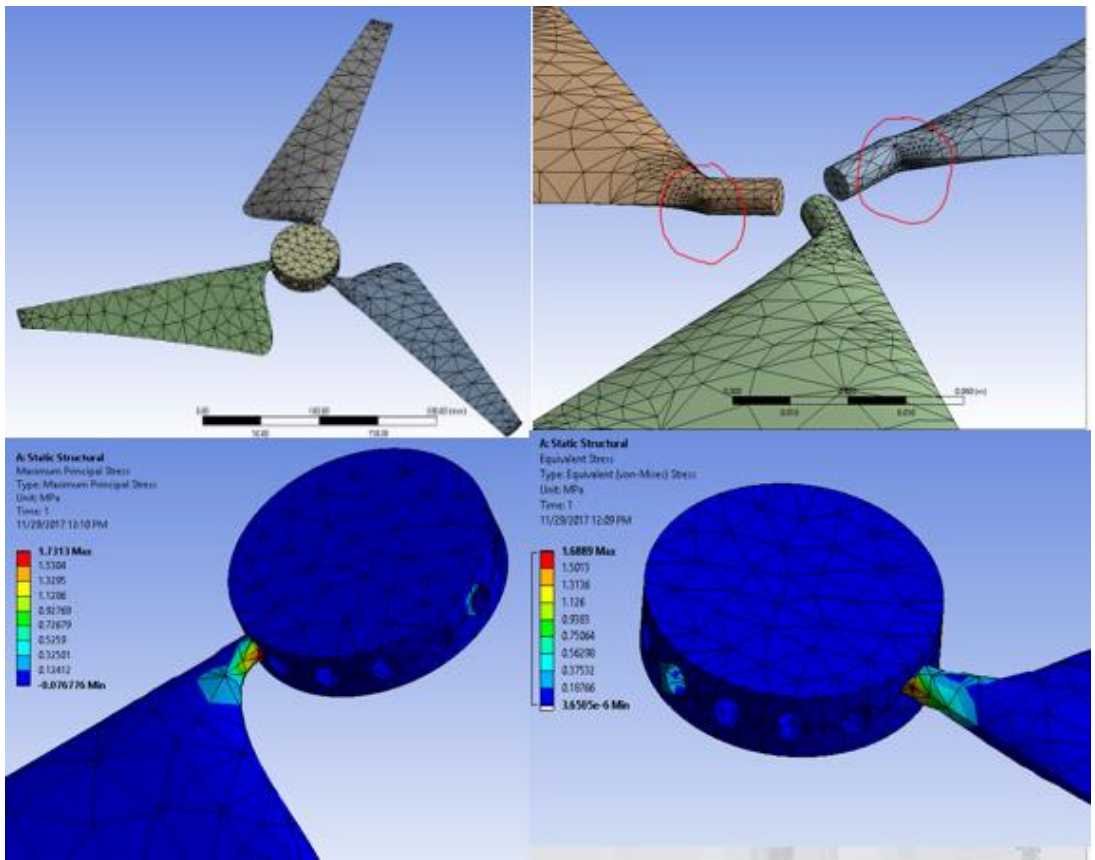
Figure 4.3. Blades Structural Behavior and Manifestation of External forces
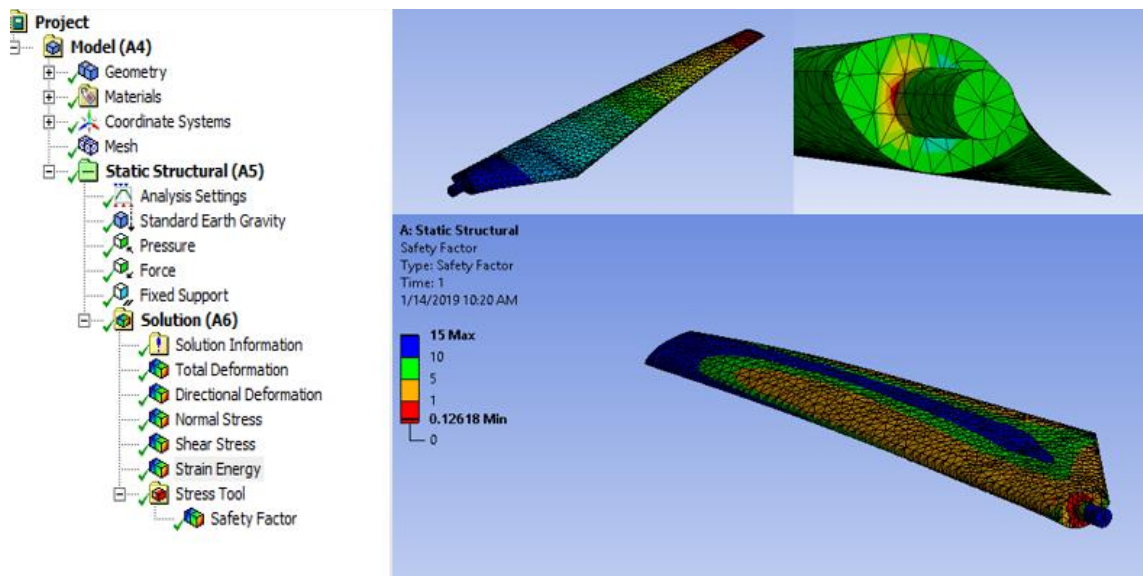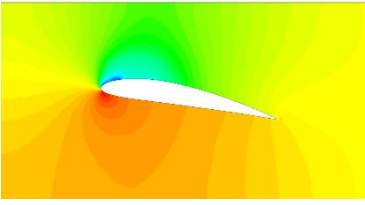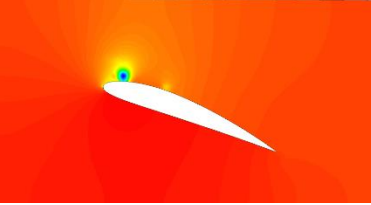
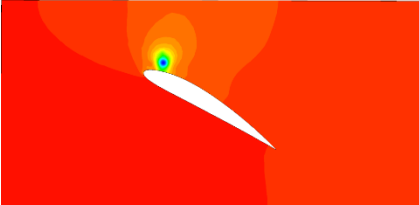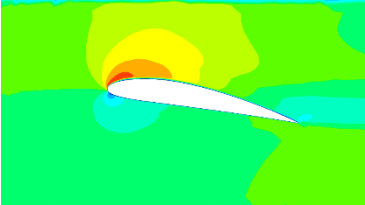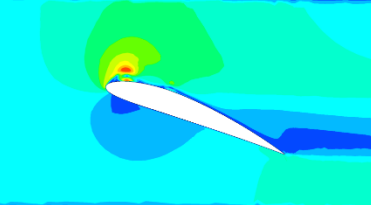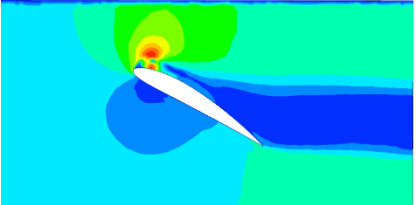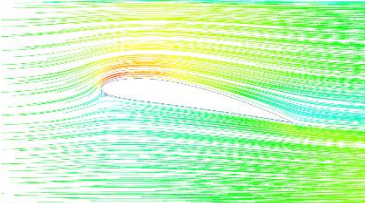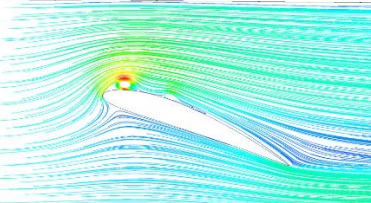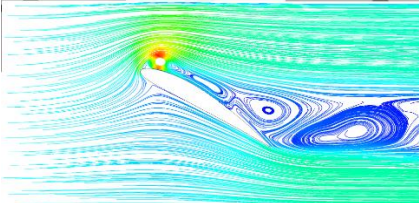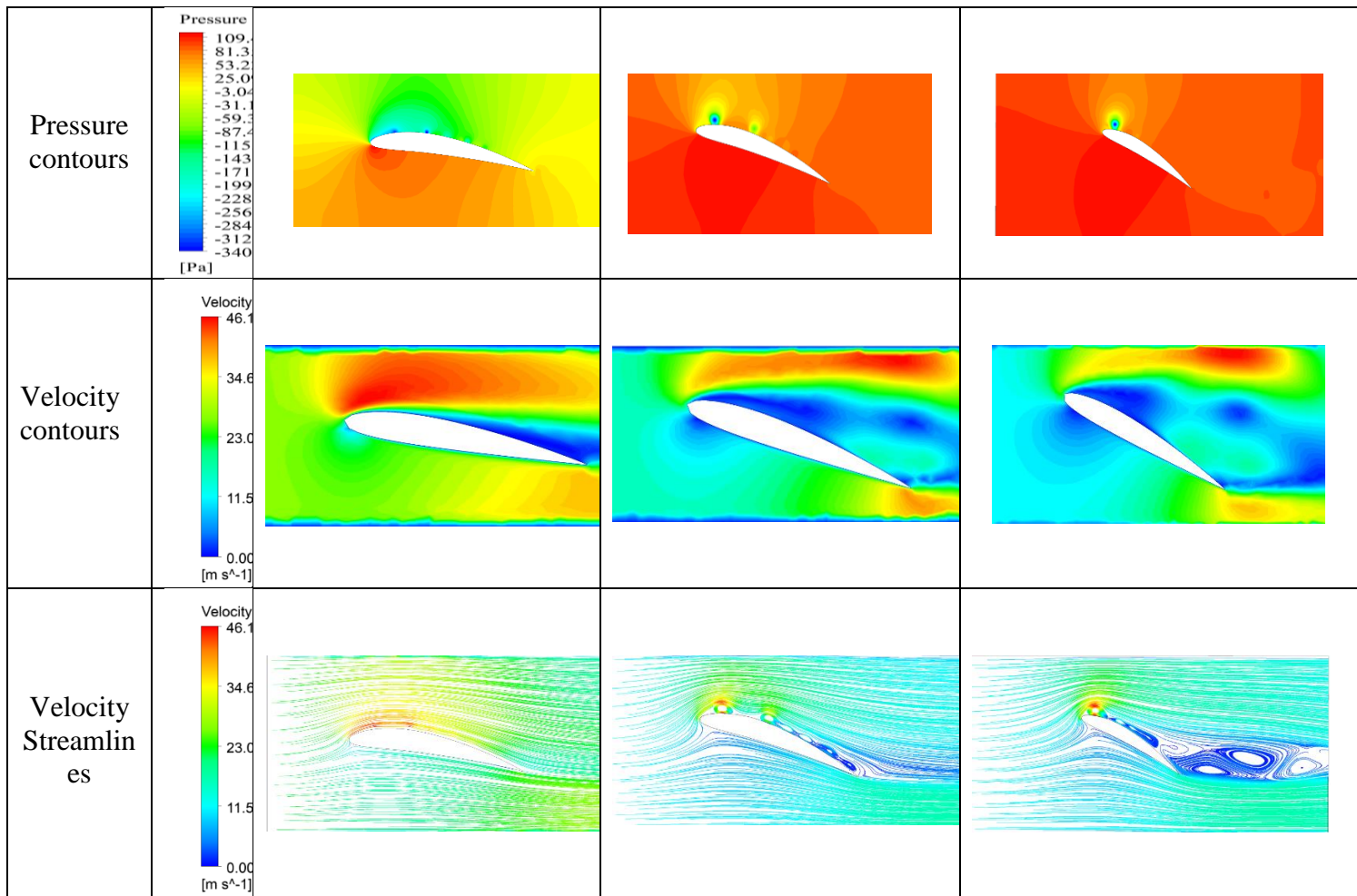**Figure 4.4. Blade potential eras of failure and safety factor**

**Table 4.3. Air Pressure Contours surrounding the Airfoils**

Air distribution type	Scale NACA 4412	10°	20°	30°
Pressure contours				
Velocity Contours				
Velocity Streamlines				
Air distribution type	Scale NACA 0018	10°	20°	30°

Pressure contours			
Velocity contours			
Velocity Streamlines			

From the CFD simulation generated, the pressure distribution can be observed around each airfoil. Higher pressure is noticed at the front and tip of the blades. The pressure distribution associated with the lift and drag coefficients justified the shown pressure distribution profile across the airfoils and therefore around the blades. Shown in the graphs below are the lift versus the drag coefficients and in order to obtain some numerical value of the lift force, an expression

was generated in the post-processing to define the lift force generated by each blade.
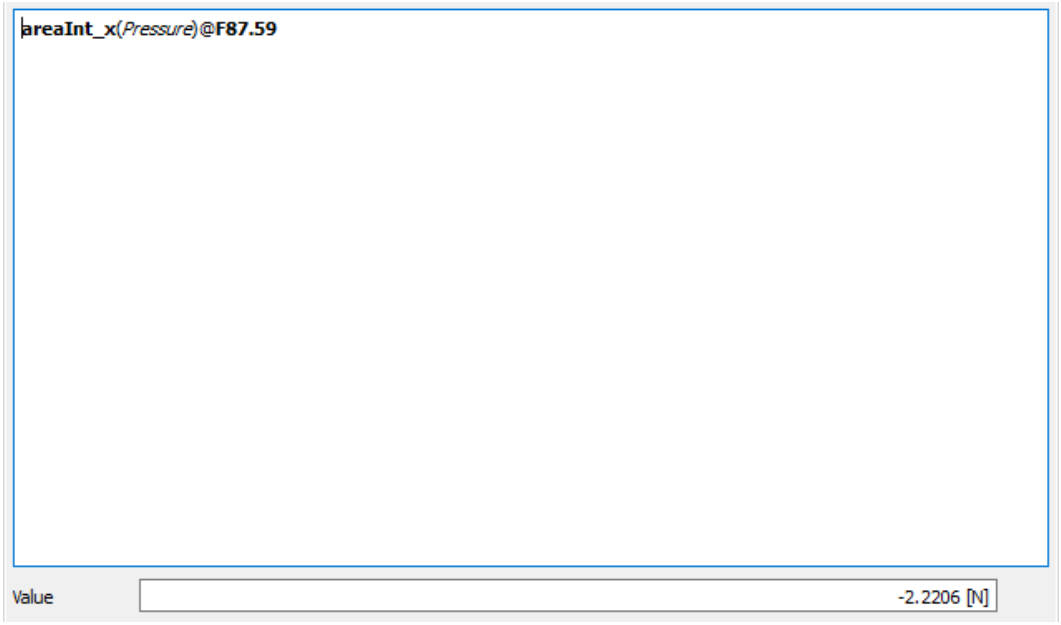
Moreover, a graph was generated to clearly observe the trend of the pressure distribution

and in the same way estimate the lift coefficient and therefore the lift force.
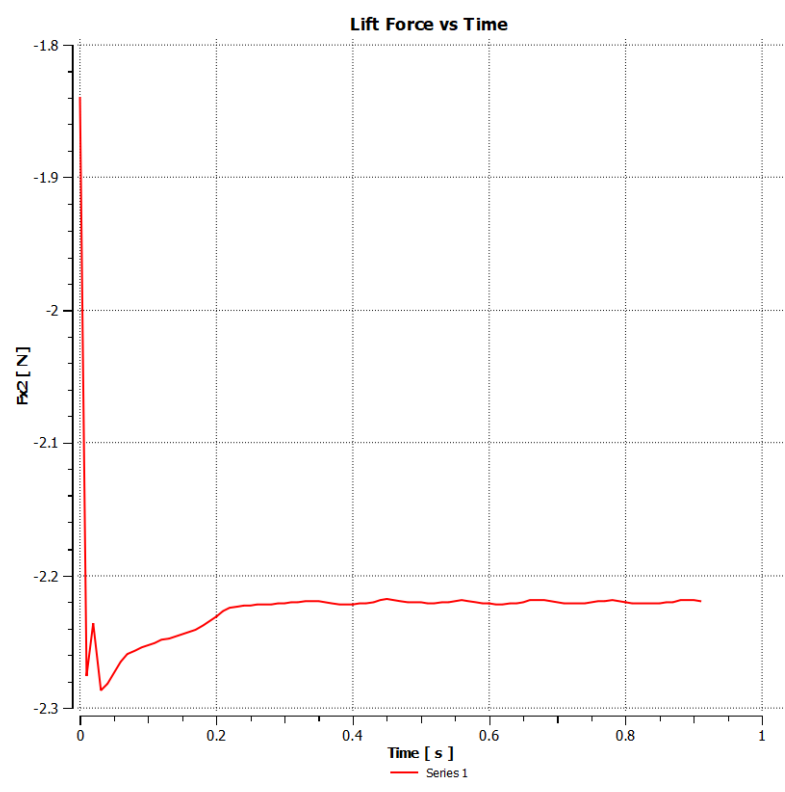
As predicted, with less drag and high lift coefficient, the maximum velocity occurred at the tip of the blades and this can be justified by the concept of relative velocity and position of the blade (tilted manner) which is aligned with the relative wind speed. In addition, as the blade velocity increases to the tip, the relative wind speed becomes more inclined toward the tip. Therefore, it can be concluded that there is a continuous twist in the blade. Another thing that will need a closer look is the pressure distribution around the blades. As detailed in the table below, it can be noticed that the pressure is lower on the back surface of the blades compared to the front and the pressure difference between the front and the back generate the lift. Also, from the plane showing the pressure distribution, it is easy to locate where the higher pressures are.

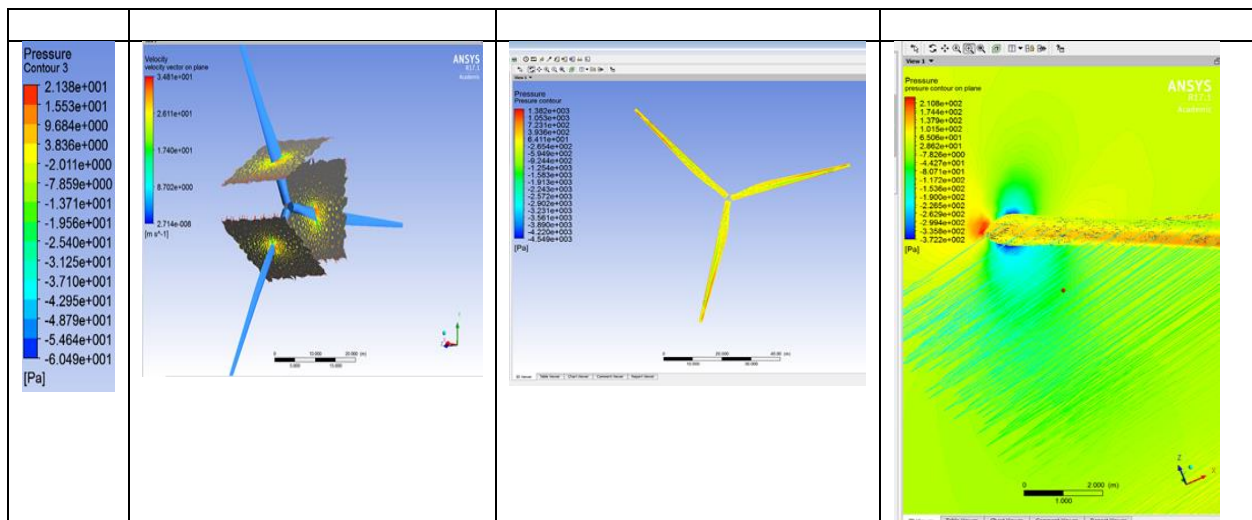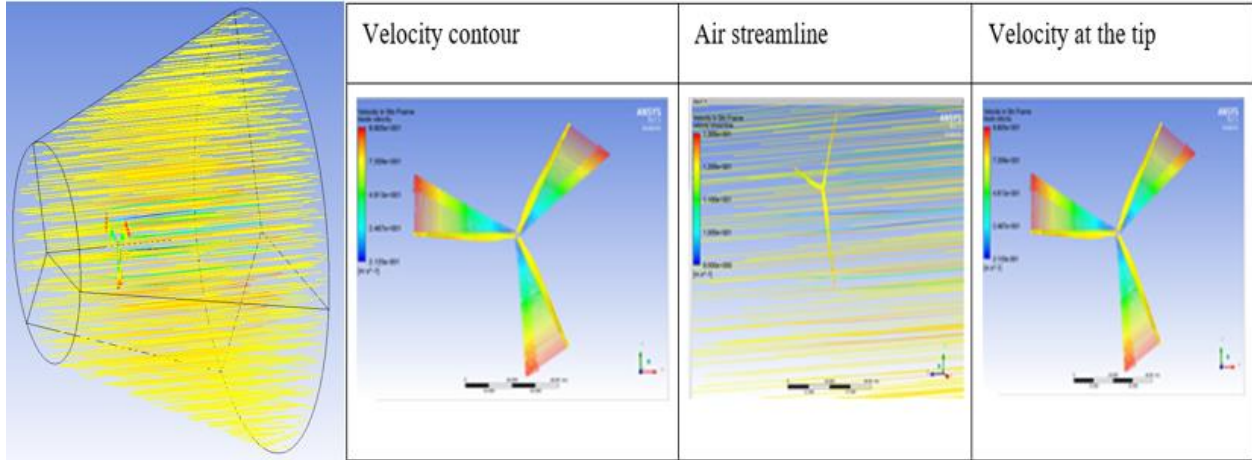**Figure 4.5 Pressure contours surrounding blades**

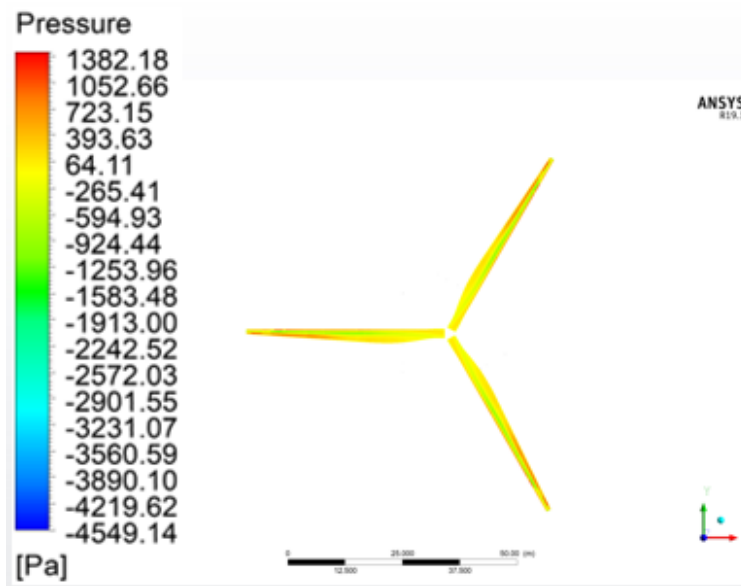**Figure 4.6. Velocity contours surrounding blades**
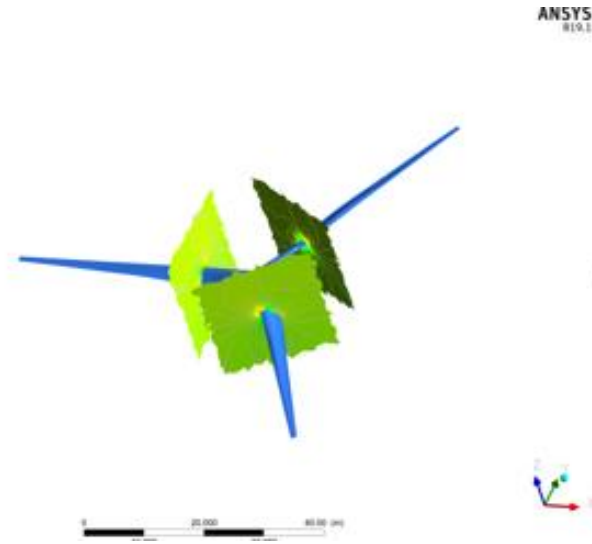

Figure 4.7. Blade pressure contour

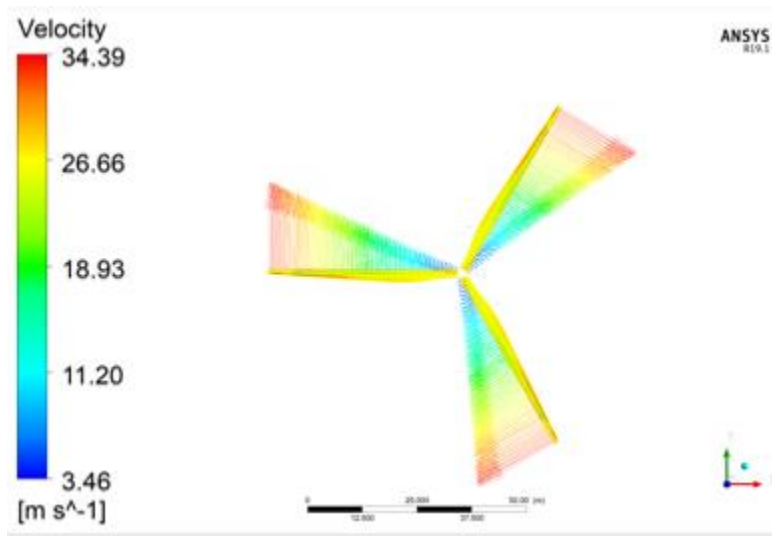**Figure 4.8. On plane pressure contour**

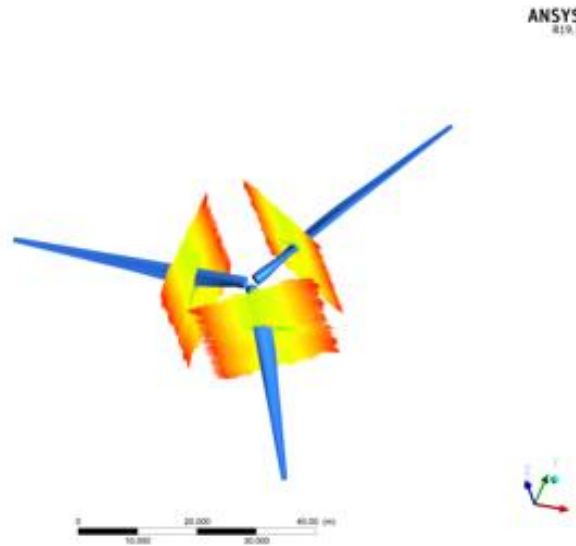**Figure 4.9. Velocity distribution per unit length**

ANSYS
R19.1

Figure 4.10. On plan local velocity contour

This section contains the pressure contours surrounding the blades of the helical models. The cross-sections vary in the y-direction due to the blade twist. Three planes were created in the post-processing for viewing the results. The planes are located at the top, middle, and bottom of each model and are shown in figure 4.8 and figure 4.10.

4.3 Experimental Results

For all experimental results presented, a minimum of 370 data points were collected within each of the 21 trials respectively at 10°, 20°, 30° of blade angle of attack and at 4, 6, 8 m/s of wind speed. In terms of the Rayleigh distribution of wind speed, a wind turbine blade characterization is based on the best power performance. For research objective purposes, the experimental set up is for low wind speed, where the prevailing wind speed is considered to be in the range of 4m/s and 8 m/s. With the 7 blades created using different airfoils from NACA 0010 to NACA 2414 and combining several airfoils in one blade design, the results indicate that the rotor exhibits higher power output when the wind speed increases and reaches 8 m/s for all blades; however, the

disparity between the power outputs for each blade clearly indicates the best fit airfoil type to be used in a blade design for low wind speed conditions. Based on figure 12, to harvest the maximum power in a region with low wind speed, a blade design must consider using NACA 6412 or NACA 2414 because the comparison of the experimental results in figure 12 indicated that these two airfoils used in the blade design generated a significant amount of power as opposed to the 5 other airfoils selected.
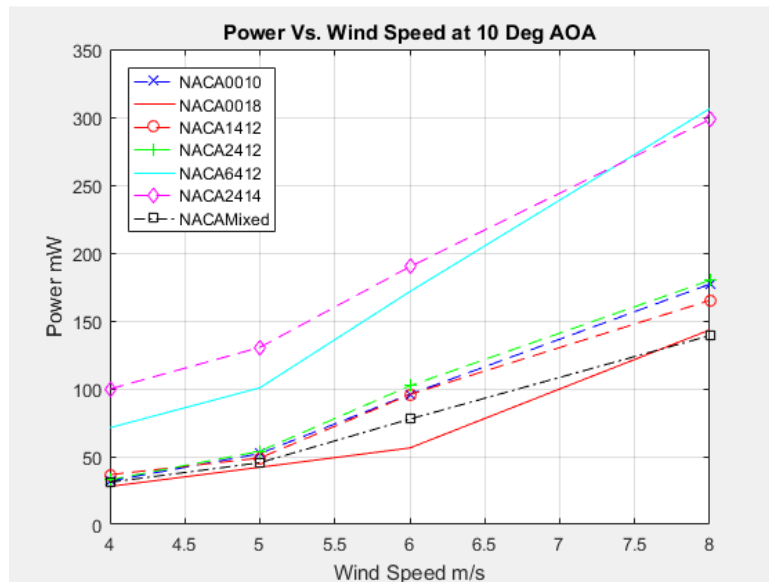
Figure 4.11. Power vs. Wind speed at 10°

Similar to figure 12, figure 13 and 14 displayed that as the wind speed increased, the power also increased and by comparing the power generated by each blade, the choice of NACA 6412 and NACA 2414 is confirmed as the best choice of airfoil type in the blade design for low wind speed region. However, by observation of these figures (12, 13 and 14), there was a decrease in the power generated when the angle changed from 10°, 20° and 30°. Figures 12, 13 and 14 demonstrate that at 10°, AOA exhibits better power performance than 20° and 30° AOA. It can be concluded that for better performance, a wind turbine blade must be set at its optimum angle of attack.

Figure 4.12. Power vs. Wind speed at 20°

Figure 4.13. Power vs. Wind Speed at 30°

CHAPTER 5

CONCLUSIONS AND RECOMMENDATIONS

5.1 Summary of work

The present research investigates the experimental and numerical of the aerodynamic performance for the horizontal-axis wind turbine model with various blade designs. Four different models 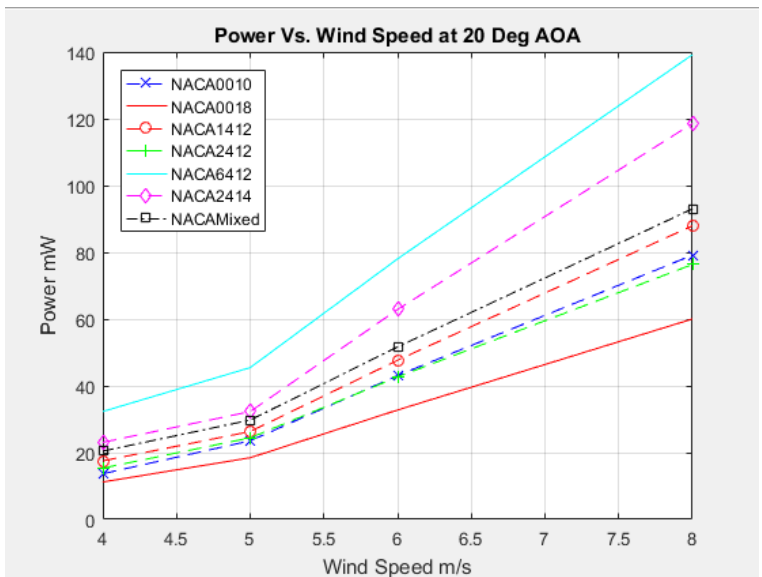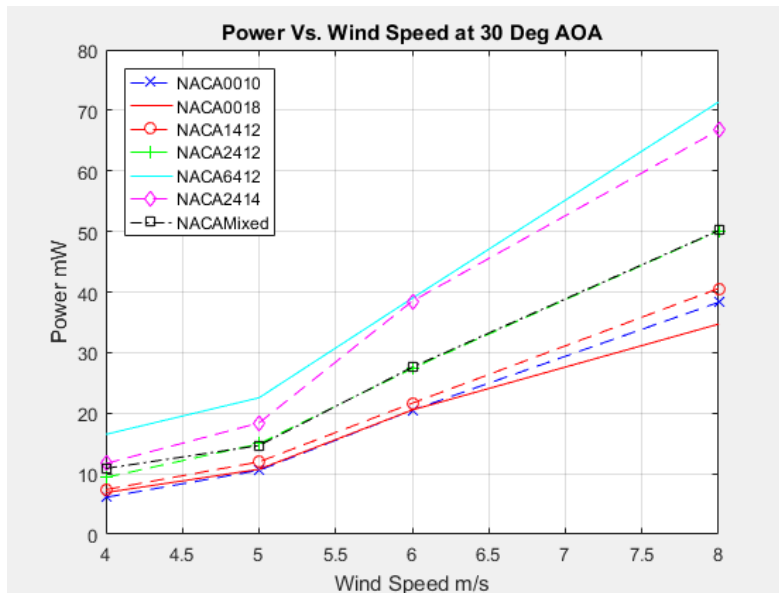are used in this investigation: four airfoils are selected to create the blade models with improving the blades' structural geometries and a combination of airfoil blade models at a17.5 degree angle of twist. All HAWT CAD models are designed via SolidWorks commercial software, and the physical models are 3D printed using FDM and SLA technologies. Additionally, ANSYS Fluent simulations are performed to validate the concepts for the blade models and then the experimental data is used to input the boundary conditions of the 3D numerical simulations.

5.2 Conclusions

The following conclusions can be drawn from this study:

● In the concept of the HAWT blade design, selecting the right airfoil type plays a huge role in the power generation of a system.

● For efficiency purposes, the design must carefully select the airfoil type.

● The blade shape and design improves the power generation of the turbine.

As stated above in the hypothesis: If the power production of a turbine is intrinsically dependent on the blade design, then by variating the airfoil types in the design, the power generation from the wind turbine should considerably experience an important increase of the overall performance.

REFERENCES

C.J. Bai, F.B. Hasiao, G. S. Mowry, M.H. Li, G. Y. Huang, and Y. J. Chen. 2013. "Design of Horizontal-Axis Wind Blade and Aerpdynamic Investigation using numerical Simulation Turbine." *Journal of Renewable & Sustainable Energy* 3, no. 3: 033109. *Academic Search Complete*, EBSCO*host* (accessed November 3, 2016).

Alaimo, Andrea, Antonio Esposito, Antonio Messineo, Calogero Orlando, and Davide Tumino. 2015. "3D CFD Analysis of a Vertical Axis Wind Turbine and Horizontal Axis wind Turbine." *Energies (19961073)* 8, no. 4: 3013-3033. *Academic Search Complete*, EBSCO*host* (accessed March 6, 2016).

Altan, Burçin Deda, and Mehmet Atılgan. 2008. "An experimental and numerical study on the improvement of the performance of Savonius wind rotor." *Energy Conversion & Management* 49, no. 12: 3425-3432. *Academic Search Complete*, EBSCO*host* (accessed November 9, 2014).

ANSYS Fluent Theory Guide—ANSYS Release Version 15.0, User's Guide; ANSYS Inc.: Canonsburg, PA, USA, 2012.

Armstrong, Shawn, Andrzej Fiedler, and Stephen Tullis. 2012. "Flow separation on a high Reynolds number, high solidity vertical axis wind turbine with straight and canted blades and canted blades with fences." *Renewable Energy: An International Journal* 41, 13-22. *Academic Search Complete*, EBSCO*host* (accessed November 9, 2014).

Bachu, Deb, Gupta Rajat, and Misra R. D. 2013. "PERFORMANCE ANALYSIS OF A HELICAL SAVONIUS ROTOR WITHOUT SHAFT AT 45° TWIST ANGLE USING CFD." *Journal Of Urban & Environmental Engineering* 7, no. 1: 126-133. *Environment Complete*, EBSCO*host* (accessed March 9, 2016).

Bashar, Mohammad M., Rahman, and Khan. 2013. "Computational Studies on the Flow Field of Various Shapes-Bladed Vertical Axis Savonius Turbine in Static Condition." *ASME 2013 International Mechanical Engineering Congress and Exposition*. San Diego, CA, USA, November 15-21, 2013.

Beri, Habtamu, and Yao Yingxue. 2011. "Numerical Simulation of Unsteady Flow to Show Self-starting of Vertical Axis Wind Turbine Using Fluent." *Journal Of Applied Sciences* 11, no. 6: 962-970. *Engineering Source*, EBSCO*host* (accessed November 9, 2014).

Bhuyan, S., and A. Biswas. 2014. "Investigations on self-starting and performance characteristics of simple H and hybrid H-Savonius vertical axis wind rotors." *Energy Conversion & Management* 87, 859-867. *Academic Search Complete*, EBSCO*host* (accessed November 3, 2014).

Can, Kang, Yang Xin, and Wang Yuli. 2013. "Turbulent Flow Characteristics and Dynamics Response of a Vertical-Axis Spiral Rotor." Energies (19961073) 6, no. 6: 2741-2758. Academic Search Complete, EBSCOhost (accessed March 8, 2016).

Deb, Bachu, Rajat Gupta, and R. D. Misra. 2014. "Experimental Analysis of a 20° Twist Helical Savonius Rotor at Different Overlap Conditions." *Applied Mechanics & Materials*no. 592-594: 1060-1064. *Engineering Source*, EBSCO*host* (accessed March 6, 2016).

Díaz, Palencia, Argemiro, Giovanni Jiménez Pajaro, and Khriscia Utria Salas. 2015. "Computational model of Savonius turbine." *INGENIARE - Revista Chilena De Ingeniería*23, no. 3: 406-412. *Academic Search Complete*, EBSCO*host* (accessed March 6, 2016).

FLUENT Manual—ANSYS Release Version 15.0, User's Guide; ANSYS Inc.: Canonsburg, PA, USA, 2012.

Gavaldà, Jna., J. Massons, and F. Díaz. 1990. "Experimental study on a self-adapting Darrieus—Savonius wind machine." *Solar And Wind Technology* 7, 457-461. *ScienceDirect*, EBSCO*host* (accessed November 9, 2014).

Ghatage, Swapnil V., and Jyeshtharaj B. Joshi. 2012. "Optimisation of vertical axis wind turbine: CFD simulations and experimental measurements." *Canadian Journal Of Chemical Engineering* 90, no. 5: 1186-1201. *Engineering Source*, EBSCO*host* (accessed November 9, 2014).

Gorelov, D., and V. Krivospitsky. 2008. "Prospects for development of wind turbines with orthogonal rotor." *Thermophysics & Aeromechanics* 15, no. 1: 153. *Publisher Provided Full Text Searching File*, EBSCO*host* (accessed November 5, 2014).

Gupta, R., A. Biswas, and K.K. Sharma. 2008. "Comparative study of a three-bucket Savonius rotor with a combined three-bucket Savonius–three-bladed Darrieus rotor." *Renewable Energy: An International Journal* 33, no. 9: 1974-1981. *Academic Search Complete*, EBSCO*host* (accessed November 5, 2014).

Islam, Mazharul, David S.-K. Ting, and Amir Fartaj. 2008. "Aerodynamic models for Darrieus-type straight-bladed vertical axis wind turbines." *Renewable & Sustainable Energy Reviews* 12, no. 4: 1087-1109. *Academic Search Complete*, EBSCO*host* (accessed November 9, 2014).

Jeon, Keum Soo, Jun Ik Jeong, Jae-Kyung Pan, and Ki-Wahn Ryu. 2014. "Effects of end plates with various shapes and sizes on helical Savonius wind turbines." *Renewable EnergyScienceDirect*, EBSCO*host* (accessed March 6, 2016).

Kamoji, M.A., S.B. Kedare, and S.V. Prabhu. 2009. "Performance tests on helical Savonius rotors." *Renewable Energy* 34, 521-529. *ScienceDirect*, EBSCO*host* (accessed March 10, 2016).

Kou, Wei, Xinchun Shi, Bin Yuan, and Lintao Fan. 2011. "Modeling analysis and experimental research on a combined-type vertical axis wind turbine." *2011 International Conference On Electronics, Communications & Control (ICECC)* 1537. *Publisher Provided Full Text Searching File*, EBSCO*host* (accessed November 3, 2014).

Lee, Jae-Hoon, Young-Tae Lee, and Hee-Chang Lim. 2016. "Effect of twist angle on the performance of Savonius wind turbine." *Renewable Energy* 89, 231-244. *ScienceDirect*, EBSCO*host* (accessed March 8, 2016).

MacPhee, David, and Asfaw Beyene. 2012. "Recent Advances in Rotor Design of Vertical Axis Wind Turbines." *Wind Engineering* 36, no. 6: 647-666. *Environment Complete*, EBSCO*host* (accessed November 3, 2014).

Mohamed, M.H. 2012. "Performance investigation of H-rotor Darrieus turbine with new airfoil shapes." *Energy* 47, no. 1: 522-530. *Academic Search Complete*, EBSCO*host* (accessed November 9, 2014).

Morshed, K. N., M. Rahman, G. M. and M. Ahmed, Wind Tunnel Testing and Numerical Simulation on Aerodynamic Performance of a Three Bladed Savonius Wind Turbine," International Journal of Energy and Environmental Engineering, 2013, pp. 4-18.

Pope, K., G. F. Naterer, I. Dincer, and E. Tsang. 2011. "Power correlation for vertical axis wind turbines with varying geometries." *International Journal Of Energy Research* 35, no. 5: 423-435. *Environment Complete*, EBSCO*host* (accessed November 9, 2014).

Ricci, Renato, Roberto Romagnoli, Sergio Montelpare, and Daniele Vitali. 2016. "Experimental study on a Savonius wind rotor for street lighting systems." *Applied Energy* 161, 143-152. *Environment Complete*, EBSCO*host* (accessed March 10, 2016).

Rui-Tao, Deng, Song Lei, Yang Zong-Xiao, Yang Hang-Hang, and Wang Long-Biao. 2011. "Research and development of a simple straight-flow wind tunnel test equipment for vertical axis wind turbines." *International Conference On Advanced Mechatronic Systems (Icamechs), 2011* 250. *Publisher Provided Full Text Searching File*, EBSCO*host* (accessed November 7, 2014).

Sagol E, Reggio M, Ilinca A. "Assessment of Two-Equation Turbulence Models and Validation of the Performance Characteristics of an Experimental Wind Turbine by CFD." *ISRN Mechanical Engineering* [serial online]. January 2012; 1.

Saha, U.K., and M. Jaya Rajkumar. 2006. "On the performance analysis of Savonius rotor with twisted blades." *Renewable Energy* 31, 1776-1788.*ScienceDirect*, EBSCO*host* (accessed March 9, 2016).

Saha, U., Thotla, S., & Maity, D. (2008). "Optimum design configuration of Savonius rotor through wind tunnel experiments." *Journal Of Wind Engineering & Industrial Aerodynamics*, *96*1359-1375. doi:10.1016/j.jweia.2008.03.005

Wenehenubun, Frederikus, Andy Saputra, and Hadi Sutanto. 2015. "An Experimental Study on the Performance of Savonius Wind Turbines Related With The Number Of Blades." Energy Procedia 68, no. 2nd International Conference on Sustainable Energy Engineering and Application (ICSEEA) 2014 Sustainable Energy for Green Mobility: 297-304. ScienceDirect, EBSCOhost (accessed March 9, 2016).

"Wind Vision: A New Era for Wind Power in the United States." ENERGY.GOV. Accessed April 7, 2016. http://energy.gov/eere/wind/maps/wind-vision.

APPENDICES

Appendix A: Improvements to the GSU Wind Tunnel

The improvement to the mechanical engineering department wind energy laboratory is the addition of a new test section for more accurate data collection using the existing wind tunnel. The data acquisition system was built by Relwinde F.W. Zongo (graduate student) and the collaboration of Robben Callaghan (under-graduate) using the resource in the machine shop on campus. The first step consisted of purchasing equipment (Energy sensor, variable load, the data collector software), shown in figure 1B. In addition, figure 2B represents the building process of the system mainframe.

Figure 1A. Wind Energy Lab Data Acquisition Subsystem

Figure 2A. Construction of the Data Acquisition Mainframe

After the completion of the construction of the mainframe, the frame was moved to the wind energy research lab. Displayed in Figure 3B shows the new completed data collection section.

Figure 3A. Completed Data and Test Section Frame on Caster

An ongoing project to build an additional HAWT testing new fixture for specifically blade design optimization testing. The CAD model of the entire assembly can be seen in figure 4B. To design this system, it was broken down into two systems. The design of the housing unit and the electrical circuits system. The housing unit was made from an old data housing structure. It was cut up using a handheld the cutting wheel. Once cut apart it was measured and welded together to represent the shape of a dolly. The bottom of the housing unit uses sheet metal that was bent and welded to the frame in order to sit the inverter and batteries in the unit.
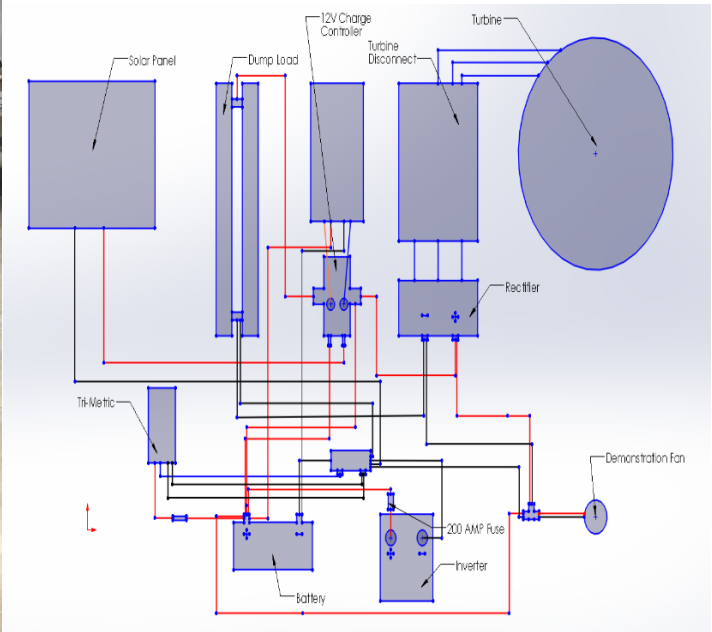
Figure 4A. CAD and Fabricated Model of New HAWT Blades Design Testing Unit.
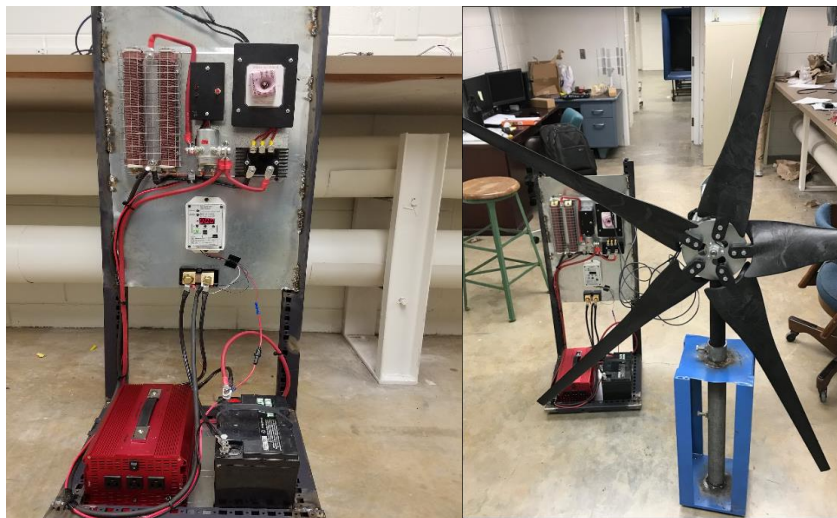
Circuit Connected to Wind Turbine

Full Hybrid System Set Up

Complete System Wiring Diagram